Estimating Waiting Distances Between Genealogy Changes under a Multi-Species Extension of the Sequentially Markov Coalescent

Patrick F. McKenzie[1] and Deren A. R. Eaton[1,*]

[1] *Department of Ecology, Evolution, and Environmental Biology, Columbia University, New York, NY 10027, USA*

[*] *Contact: de2356@columbia.edu*

Keywords: Recombination, Phylogeny, SMC, Gene Tree, Species Tree, Concatalescence, ARG

Abstract

Genomes are composed of a mosaic of segments inherited from different ancestors, each separated by past recombination events. Consequently, genealogical relationships among multiple genomes vary spatially across different genomic regions. Genealogical variation among unlinked (uncorrelated) genomic regions is well described for either a single population (coalescent) or multiple structured populations (multispecies coalescent). However, the expected similarity among genealogies at linked regions of a genome is less well characterized. Recently, an analytical solution was derived for the distribution of the waiting distance for a change in the genealogical tree spatially across a genome for a single population with constant effective population size. Here we describe a generalization of this result, in terms of the distribution of waiting distances between changes in genealogical trees and topologies for multiple structured populations with branch-specific effective population sizes (i.e., under the multispecies coalescent). We implemented our model in the Python package *ipcoal* and validated its accuracy against stochastic coalescent simulations. Using a novel likelihood framework we show that tree and topology-change waiting distances in an ARG can be used to fit species tree model parameters, demonstrating an application of our model for developing new methods for phylogenetic inference. The Multi-Species Sequentially Markov Coalescent (MS-SMC) model presented here represents a major advance for linking local ancestry inference to hierarchical demographic models.

1 Introduction

The multispecies coalescent (MSC) is an extension of the coalescent (Kingman, 1982), a model that describes the distribution of genealogical histories among gene copies from a set of sampled individuals. Whereas the coalescent models a single panmictic population, the MSC includes constraints that prevent samples in different lineages from sharing a most recent genealogical ancestor until prior to a population divergence event that separates them (Maddison, 1997; Maddison & Knowles, 2006). Conceptually, the MSC can be viewed as a piecewise model composed of the standard coalescent applied to each interval of a "species tree" representing the relationships and divergence times among isolated lineages. Genealogies are constrained to be embedded within species trees, and the joint likelihood of MSC model parameters can be calculated from the coalescent times among a distribution of sampled genealogies (Degnan &

Rosenberg, 2009; Rannala & Yang, 2003). In both the coalescent and MSC models, effective population size (N_e) is the key parameter determining the rate of coalescence and can vary across different lineages.

Importantly, both the single-population coalescent and the MSC specify the distribution of *unlinked* (uncorrelated) genealogies. By contrast, two linked genealogies that are drawn from nearby regions of a genome are expected to be more similar than two random draws under these models. This spatial autocorrelation is a consequence of shared ancestry among samples at nearby regions, which decays over time and distance as recombination events reduce their shared ancestry. To be clear, the spatial correlation here refers to the similarity among neighboring genealogies on a chromosome, and not to the similarity of genomes in geographic space. As a data structure, an ordered series of linked genealogies and the lengths of their associated intervals on a chromosome (Fig. 1) is represented by an ancestral recombination graph (ARG) (Griffiths & Marjoram, 1996), or similarly, a tree-sequence (Kelleher *et al.*, 2016) (hereafter we will refer to it generically as an ARG).

An algorithm to stochastically generate ARGs under the coalescent with recombination was developed early on by Hudson (1983) and later extended as a spatial algorithm by Wiuf & Hein (1999b). This latter process models the difference between sequential genealogies by randomly detaching an edge from a genealogy and sampling a waiting time (based on the coalescent rate) until it reconnects to the genealogy at a different shared ancestor. Thus, under this spatial model, a set of samples effectively substitutes one ancestor for another on either side of each recombination breakpoint. Implicit to this algorithm is the assumption that recombination occurs at some predictable rate (or rate map) from which the waiting distance between recombination events can be modeled as an exponentially distributed random variable (Wiuf & Hein, 1999b). Although generating ARGs consistent with a demographic model is relatively simple under this process, inferring an ARG from sequence data – composing a set of recombination breakpoints and local genealogy inferences – remains highly challenging (Brandt *et al.*, 2022). This stems in part from the great complexity of this problem but also reflects limitations of our current models for extracting historical information from linked genome data.

A major advance was achieved through development of the sequentially Markov coalescent (SMC), a simpler approximation of the coalescent with recombination that restricts the types of recombination events that can occur (McVean & Cardin, 2005). Specifically, an edge that is detached from a genealogy by recombination is allowed only to re-coalesce with ancestral lineages that contributed genetic material to samples in that interval (as opposed to re-coalescing with any ancestral lineage). This greatly reduces the space of possible ARGs without changing the distribution of sequential genealogies, and in doing so it enables modeling changes between sequential genealogies as a Markov process (McVean & Cardin, 2005). Under these assumptions a tractable likelihood framework can be developed. Because neither genealogies nor segment lengths can be observed directly, most SMC-based inference methods use a hidden Markov model (HMM) to treat these as hidden states that influence observable changes in sequence data (Spence *et al.*, 2018). Examples of inference tools built on the SMC framework include PSMC (Li & Durbin, 2011) and MSMC (Schiffels & Durbin, 2014) which use pairwise coalescent times between sequential genealogies to infer changes in effective population sizes through time, and ARGweaver (Hubisz & Siepel, 2020; Rasmussen *et al.*, 2014), which infers ARGs from genome alignments using an SMC-based conditional sampling method.

Marjoram & Wall (2006) described an important extension to the SMC, termed the SMC', for addi-

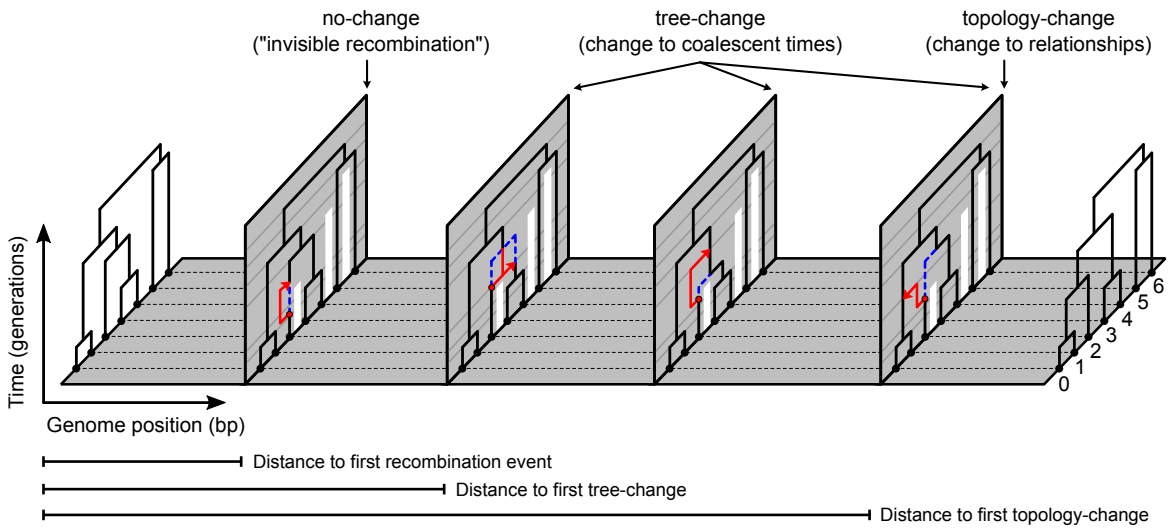

Figure 1. An ancestral recombination graph (ARG) is composed of a series of genealogies each spanning non-overlapping intervals of a genome separated by recombination breakpoints. Here, four recombination breakpoints separate interval start and end positions along a small chromosome alignment. The individual genealogies represent the history of a set of 7 samples constrained by a 4-tip species tree model (as in Fig. 2). Recombination events are indicated by vertical panels. Each shows the SMC' process by which a subtree (below the red circle) is detached and then re-coalesces (red arrow) with one of the remaining lineages. The former edge (blue dotted) which existed throughout the interval to the left of a panel is replaced by a new edge (red) through the subsequent interval. Vertical bars (white) represent barriers to coalescence between samples in different species tree intervals (MSC model lineages). Four categories of recombination events are shown from left to right, representing different outcomes based on the lineage with which a detached subtree re-coalesces. These are grouped more generally into three *event types*: (1) no-change, (2) tree-change, and (3) topology-change. Every recombination event causes either a no-change or tree-change event, whereas topology-change events are a subset of possible tree-change events. The expected waiting distance until a specific recombination event type occurs can be calculated under the MS-SMC given a starting genealogy, MSC model, and recombination rate.

tionally modeling "invisible" recombination events, in which a detached lineage re-attaches with its own ancestral lineage prior to the time of that lineage's next coalescent event. This leads to no change between the genealogies in two sequential genomic intervals despite the occurrence of a recombination event between them. The inclusion of such events has been shown to significantly improve inference methods (Wilton *et al.*, 2015). Under the SMC', a detached lineage can thus re-coalesce with an allowable ancestral lineage over a continuous range of time, leading to one of four possible categorical patterns for the relationship between two sequential genealogies (Fig. 1, Fig. S1): (1) no change; (2) shortening of a coalescent time; (3) lengthening of a coalescent time; and (4) a change to the genealogical topology (relationships). These can be grouped more generally into three types: "no-change" (category 1), "tree-change" (categories 2-4), and "topology-change" (category 4). Recently, Deng *et al.* (2021) derived a set of solutions for the waiting distances to each of these three types of outcomes for a single population with constant effective population size. This provided an important advance by establishing a neutral expectation not only for the distance until the next recombination event occurs, but more specifically, for the distance until differ-

ent categorical types of recombination events occur. Such events leave different detectable signatures in sequence data and extend across different spatial distances of the genome, thus extending the scale over which information from spatial genealogical patterns can be extracted from genomes.

Here, we extend the theory of Deng *et al.* (2021) to an MSC framework to derive the distribution of the waiting distance until different types of genealogy changes occur under a parameterized species tree model. The waiting distances between recombination events that cause topology-change may be of greatest interest, as they leave the most detectable signatures in sequence data and are relevant to expected gene tree distributions that form an important component of many MSC-based methods (Baum, 2007; Degnan & Rosenberg, 2009; Knowles & Kubatko, 2011). The waiting distance between topology-change events may include multiple intervening recombination events of the no-change or tree-change type (Fig. 1). The relative occurrence of events that do not result in topology changes can be especially high in small sample sizes (Wilton *et al.*, 2015), which are common in MSC-type datasets in which samples are partitioned among species tree intervals. Since the partitioning of coalescent events among species tree intervals is expected to constrain the types of recombination events that will be observed, the distributions of waiting distances between different types of genealogy changes should be highly dependent on, and thus informative about, the species tree model. We refer to the general framework of embedding the SMC' in an MSC model as the MS-SMC.

2 Approach

2.1 Comparison to Deng *et al.* (2021)

Our approach is a generalization of the Deng *et al.* (2021) derivation of waiting distances to genealogy changes for a single population of constant size. We modified the single-population model to (1) include barriers to coalescence imposed by a species tree topology, and (2) integrate over changing coalescence rates along paths through multiple species tree intervals with different effective population sizes. In addition, we introduce a novel application of our MS-SMC model, utilizing a likelihood-based framework to estimate MSC model parameters from the waiting distances between tree-change and topology-change events in an ARG.

2.2 MSC model description

Given an MSC model ($\mathcal{S}$) composed of a species tree topology with divergence times (W) in units of generations and constant diploid effective population sizes (N_e) assigned to each branch, an embedded genealogy ($\mathcal{G}$) for any number of sampled gene copies (k) can be generated by randomly sampling coalescent times at which to join two samples into a common ancestor, starting from samples at the present in each interval. Following Kingman (1982), the probability of a coalescent event one generation in the past (reducing the number of samples from k to k-1) is given by equation 1. From this, we can model the expected waiting time ($\mathbb{E}[t_k]$) until the next coalescence event as an exponentially distributed random variable with rate parameter λ_k:

$$\lambda_k = \mathbb{P}(\text{coal event } | N_e, k) = \frac{k(k-1)}{2N_e}$$
$$and: \tag{1}$$
$$\mathbb{E}[t_k] = 1/\lambda_k$$

In a single population model with constant N_e the expected waiting time between coalescent events increases monotonically after each coalescent event, since the number of remaining samples always decreases. In an MSC model, however, the expected waiting time between coalescence events can increase or decrease through time, as the transition from one population interval to another can be associated with a different N_e value and an increase in the number of samples.

Based on this generative framework for sampling genealogies under a demographic model, the probabilities of observed genealogies can also be calculated under a demographic model. The probability of a genealogy embedded in a single population model is the product of the probability densities of each waiting time between coalescent events (Kingman, 1982). The process is similar for a genealogy embedded in a species tree model, but requires evaluating the probabilities of coalescent waiting times within each species tree interval separately – including the probability that all gene copies do not coalesce before the end of the interval (Rannala & Yang, 2003). A key feature of this framework is that for each coalescent interval with k gene copies and effective population size N_e, we can calculate the coalescent rate (λ_k) and use the exponential probability density function (Equation 2) to evaluate the likelihood of the demographic model parameters based on the distributions of coalescent times in one or more genealogies.

$$f(t_k; \lambda_k) = \lambda_k e^{-\lambda_k t_k} \tag{2}$$

2.3 MS-SMC model description and notation

Under the SMC' model, sampling of a linked genealogy requires considering not only demographic model parameters, as we did above, but also an existing genealogy – it is a method for sampling the next genealogy conditional on the previously observed one. If we define the previous genealogy as $\mathcal{G}$, and the sum of its edge lengths as $L(\mathcal{G})$, then under the assumption of a constant recombination rate through time, a recombination break point can be uniformly sampled from $L(\mathcal{G})$ to occur with equal probability anywhere on $\mathcal{G}$. A recombination event creates a bisection on a branch, separating a subtree below the cut from the rest of the genealogy (Fig. 1, Fig. S1). The subtree must then re-coalesce with an edge on the genealogy from which it was detached at a time above the recombination event. The waiting time until this re-coalescence event occurs is sampled stochastically using equation (1), where the expectation is determined by the number of samples and the effective population size.

In a single population model with constant N_e, the expected waiting time until re-coalescence increases monotonically with each coalescence event backwards in time, since each event decreases k. Once again, the MSC model differs from this: coalescent events similarly decrease k, but the merging of species tree branches into ancestral intervals increases k, and N_e can also vary among species tree intervals. Thus, the probability that a detached subtree re-coalesces to the genealogy can vary through time along its path of possible reconnection points through different species tree intervals. To calculate these probabilities,

(a)

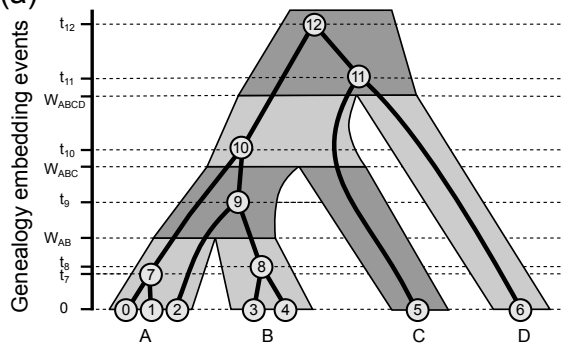

(b)

	start (σ)	end (μ)	pop	N_e (n)	N edges (k)	length (d)	branches (b)
0	0	t_7	A	N_A	3	$t_7 - 0$	0,1,2
1	t_7	W_{AB}	A	N_A	2	$W_{AB} - t_7$	2,7
2	0	t_8	B	N_B	2	$t_8 - 0$	3,4
3	t_8	W_{AB}	B	N_B	1	$W_{AB} - t_8$	8
4	0	W_{ABC}	C	N_C	1	W_{ABC}	5
5	0	W_{ABCD}	D	N_D	1	W_{ABCD}	6
6	W_{AB}	t_9	AB	N_{AB}	3	$t_9 - W_{AB}$	2,7,8
7	t_9	W_{ABC}	AB	N_{AB}	2	$W_{ABC} - t_9$	7,9
8	W_{ABC}	t_{10}	ABC	N_{ABC}	3	$t_{10} - W_{ABC}$	5,7,9
9	t_{10}	W_{ABCD}	ABC	N_{ABC}	2	$W_{ABCD} - t_{10}$	5,10
10	W_{ABCD}	t_{11}	ABCD	N_{ABCD}	3	$t_{11} - W_{ABCD}$	5,6,10
11	t_{11}	t_{12}	ABCD	N_{ABCD}	2	$t_{12} - t_{11}$	10,11
12	t_{12}	-	ABCD	N_{ABCD}	1	-	12

Figure 2. An example genealogy embedded in a species tree and the corresponding embedding table used for MS-SMC calculations. (a) A four tip species tree is composed of seven discrete population intervals separated by speciation events (W_x), each of which can be further dissected by coalescent events (t_x). (b) The probability of coalescence is constant within each discrete interval and is scaled by the number of lineages (k), the effective population size (n), and the interval length (d). Under the MS-SMC, the probability that a detached lineage will re-coalesce on a specific branch of the genealogy (e.g., branch 7) is calculated using the piecewise constant probabilities from each discrete interval spanning that branch (e.g., rows 1, 6, 7, and 8 in the embedding table).

a species tree and genealogy can be decomposed into a series of relevant intervals between events that change rates of coalescence, which we refer to as the genealogy embedding table (Fig. 2). From this table it is possible to calculate the probabilities of different recombination event type outcomes and, consequently, to model the expected waiting distances until specific recombination event types occur.

Each interval of the genealogy embedding table contains a constant number of genealogy branches (k_i) and a constant effective population size (n_i) such that the rate of coalescence is also constant. We define a number of additional variables related to this table. The length of each interval is d_i, and its lower and upper bounds are σ_i and μ_i, respectively. Similarly, the lower and upper bounds of a genealogy branch (b) are defined as t_b^l and t_b^u, respectively. An indexing variable, $\mathcal{I}_b$, is defined as the ordered set of intervals that are spanned by a specific branch of an embedded genealogy. As an example, consider genealogy branch 7 from Fig. 2a. This branch spans four intervals, labeled as rows 1, 6, 7, and 8 in the associated genealogy embedding table (Fig. 2b), and so $\mathcal{I}_7$ = {1,6,7,8}. As we will demonstrate below, this and related indexing variables will be used to calculate the probabilities of re-coalescence in different intervals, and on different branches, based on their rates of coalescence. A summary of all variables in our notation is available in table S1.

2.4 Deriving probabilities of genealogy changes in the MS-SMC

A recombination event occurring on $\mathcal{G}$ can result in three types of outcomes (Fig. 1). Of these, there is a zero-sum relationship between a no-change and tree-change event, such that one or the other must occur. Therefore, as a first step towards describing probability statements for each of these event types, we focus first on deriving the probability of a no-change event (also termed a tree-unchanged event; Fig. 3a), which is the simplest outcome. Then, from the law of total probability, we also have a result for the probability of recombination resulting in a tree-change event. Finally, to calculate the probability of a topology-change

event, we first derive a statement for the probability of a topology-unchanged event (Fig. 3d), which is the union of a no-change event and a subset of tree-change events, where the detached lineage is restricted according to which ancestral lineages it can re-coalesce with. Full detailed derivations of all solutions below are available in the Appendix of the Supplementary Materials.

2.4.1 Probability of a no-change event

We begin by assuming knowledge of when and where recombination takes place, in terms of a recombination event bisecting branch b at time t_r. For no change to occur to the genealogy, the detached subtree must re-coalesce with its original branch – either in the same interval from which it detached, or in a later interval on the same branch (Fig. 3a). If it connects to any other lineage, this will cause a change to either the tree or topology. Equation 3 describes the probability of a no-change event given a genealogy embedded in a species tree and given the timing and branch on which recombination occurs. The interval in which recombination occurs is labeled i. The first two terms describe the probability that the subtree re-coalesces during interval i on branch b (i.e., ii), while the latter term is the probability of re-coalescing during a later interval on branch b (i.e., ij). For this, we define another indexing variable $\mathcal{J}_b(i) = \{j \in \mathcal{I}_b \mid j > i\}$, for iterating over the ordered intervals above i on branch b (e.g., Fig. 3b).

$$\mathbb{P}(\text{no-change}|\mathcal{S}, \mathcal{G}, b, t_r) = \frac{1}{k_i} + f(i,i)\exp\left\{\frac{k_i}{2n_i}t_r\right\} + \sum_{j\in\mathcal{J}_b(i)} f(i,j)\exp\left\{\frac{k_i}{2n_i}t_r\right\} \tag{3}$$

This equation is simplified by use of the function $f(i,j)$ to return the piece-wise constant probabilities of re-coalescence between pairs of intervals. When j=i, this expression involves the probability of coalescing over the remaining length of interval i above t_r; when j>i it involves the probability of coalescing in interval j and not coalescing in interval i or any other intervals between i and j. For this latter process, we define another indexing variable, $\mathcal{Q}_b(i,j) = \{q \in \mathcal{I}_b \mid j > q > i\}$, for iterating over the ordered intervals above i and below j on branch b (e.g., Fig. 3c). The function $f(i,j)$ forms the core of the MS-SMC algorithm and will reappear in several later equations. For didactic purposes, a step-by-step demonstration of equation (3) is shown in Fig. S7 of the Appendix.

$$f(i,j) = \begin{cases} -\frac{1}{k_i}\exp\left\{-\frac{k_i}{2n_i}\mu_i\right\}, & \text{if } i = j \\ \frac{1}{k_j}\left(1-\exp\left\{-\frac{k_j}{2n_j}d_j\right\}\right)\exp\left\{-\frac{k_i}{2n_i}\mu_i - \sum_{q\in\mathcal{Q}_b(i,j)}\frac{k_q}{2n_q}d_q\right\}, & \text{if } i < j \\ 0, & \text{if } i > j \end{cases} \tag{4}$$

By integrating equation 3 across all times at which recombination could have occurred on branch b (assuming a uniform recombination rate through time) we obtain the probability that recombination anywhere on this branch does not change the tree:

$$\mathbb{P}(\text{no-change}|\mathcal{S}, \mathcal{G}, b) = \frac{1}{t_b^u - t_b^l}\sum_{i\in\mathcal{I}_b}\left[\frac{1}{k_i}d_i + \frac{2n_i}{k_i}\sum_{j\in\mathcal{I}_b} f(i,j)\left(\exp\left\{\frac{k_i}{2n_i}\mu_i\right\} - \exp\left\{\frac{k_i}{2n_i}\sigma_i\right\}\right)\right] \tag{5}$$

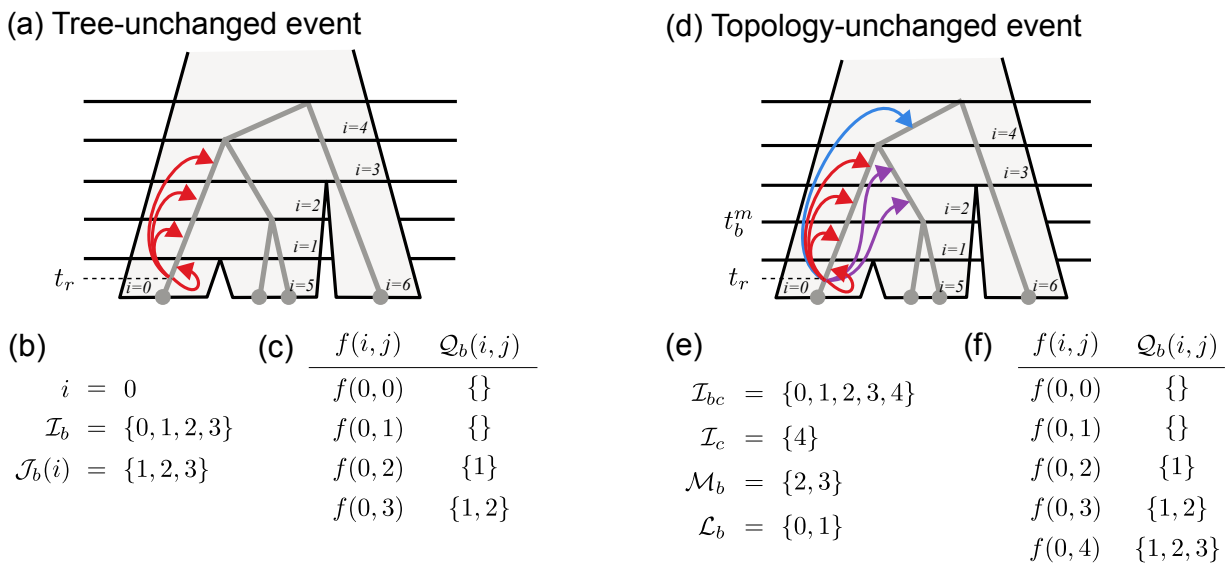

Figure 3. The probability of each categorical recombination event type is calculated from the probability of recombination occurring on a specific gene tree branch and of the resulting detached subtree re-coalescing with an available branch above that event. (a) The probability of a "no-change" (tree-unchanged) event involves re-coalescing with the same branch on which recombination occurred, for which intervals are indexed using the variable $\mathcal{I}_b$. (b) Indexing variables for calculating no-change probabilities. The indexing variable $\mathcal{I}_b$ records all intervals on branch b; the recombination event for this example occurs in interval i=0. $\mathcal{J}_b(i)$ returns all intervals in $\mathcal{I}_b$ above interval i. (c,f) The function $f(i,j)$ returns the probability that a subtree that detached in interval i will re-coalesce in interval j. This involves excluding the probability of re-coalescence in intervals between i and j, which are indexed as $\mathcal{Q}_b(i,j)$. (d) The probability of a topology-unchanged event involves re-coalescing with the same branch on which recombination occurred, or with its parent or sibling branches. (e) Additional indexing variables return intervals on the parent branch ($\mathcal{I}_c$), or branch b above ($\mathcal{M}_b$) or below ($\mathcal{L}_b$) the time (t_b^m) at which it overlaps in the same species tree interval as its sibling branch.

Finally, by summing across all branches on the tree while weighting each one by its relative proportion of edge length, we get the probability that a recombination event occurring anywhere on $\mathcal{G}$ will result in a no-change event.

$$\mathbb{P}(\text{no-change}|\mathcal{S},\mathcal{G}) = \sum_{b\in\mathcal{G}} \left[\frac{t_b^u - t_b^l}{L(\mathcal{G})}\right] \mathbb{P}(\text{no-change}|\mathcal{S},\mathcal{G},b) \tag{6}$$

2.4.2 Waiting distances to no-change and tree-change events

Under the SMC', recombination is modeled as a Poisson point process such that the time between recombination events is exponentially distributed with rate parameter λ_r: the product of the per-site per-generation recombination rate and summed branch lengths of the current genealogy (Wiuf & Hein, 1999a) (equation 7). The likelihood of an observed distance (x) between recombination events spatially along the genome, in units of base pairs, can thus be calculated from the exponential probability density function (equation 8).

$$\lambda_r = L(\mathcal{G}) \times r \tag{7}$$

$$f(x; \lambda_r) = \lambda_r e^{-\lambda_r x} \tag{8}$$

Having derived the probability that an individual recombination event is of the no-change type, we can now calculate the rate of no-change type events as a proportion of the rate of all types of recombination events. Here, waiting distances continue to be exponentially distributed. However, the new rate parameter λ_n is reduced proportionally by the probability that recombination causes no change to the genealogy (equation 9). Similarly, because a tree-change event is the opposite of a no-change event, its probability is one minus the probability of no-change (equation 10). This yields rate parameter λ_g for the exponential probability distribution of waiting distances between tree-change events.

$$\lambda_n = L(\mathcal{G}) \times r \times \mathbb{P}(\text{no-change}|\mathcal{S}, \mathcal{G}) \tag{9}$$

$$\lambda_g = L(\mathcal{G}) \times r \times (1 - \mathbb{P}(\text{no-change}|\mathcal{S}, \mathcal{G})) \tag{10}$$

2.4.3 Probability of topology-change

We next derive an analogous probability distribution for waiting distances between topology-change events. Similar to our approach for calculating tree-change probabilities as the opposite of those for a no-change (tree-unchanged) event, here we calculate topology-change probabilities as the opposite of those for a topology-unchanged event. Topology-unchanged events represent the union of all no-change events and the subset of possible tree-change events that only affect branch lengths but not the topology. Our approach for calculating these probabilities follows closely to that of Deng *et al.* (2021). In order to isolate re-coalescence events that do not change the topology, we must take into account which specific branches the detached subtree from branch b re-coalesces with. The relevant branches are its source (b), its sibling (b'), and its parent (c) (Fig. 3d). If the subtree re-coalesces with b, no change occurs; if it re-coalesces with b', the topology remains the same but a coalescent time is shortened; and if it re-coalesces with c, the topology remains the same but a coalescent time is lengthened. A re-coalescence with any other branch will change the topology.

To index over relevant intervals across the three branches on which re-coalescence can occur, we define several additional variables. The lowest time point in which both b and b' are present and exist within the same species tree interval is labeled t_b^m. For a branch b with intervals $\mathcal{I}_b$, the subset of intervals below t_b^m is $\mathcal{L}_b$, and the subset above is $\mathcal{M}_b$. The union of the sets of intervals on branches b and c is $\mathcal{I}_{bc}$ (Fig. 3e).

Once again, we begin by assuming knowledge of the branch on which a recombination event occurs and of that event's timing. This problem can be broken into two distinct cases: when t_r occurs below t_b^m, and when it occurs above t_b^m. The former requires integrating over additional intervals on b that are not shared with b'. Over all intervals on the three relevant branches, these equations use the function $f(i, j)$ to return the piecewise constant probabilities where recombination occurs in interval i and re-coalesces

in interval j (Fig. 3f). We provide a didactic example of the Equation 11 calculation in Fig. S8 of the Appendix.

$$\mathbb{P}(\text{topology-unchanged}|\mathcal{S},\mathcal{G},b,t_r) = \begin{cases} \frac{1}{k_i} + \sum_{j\in\mathcal{I}_{bc}} f(i,j)\exp\left\{\frac{k_i}{2n_i}t_r\right\} + \sum_{j\in\mathcal{M}_b} f(i,j)\exp\left\{\frac{k_i}{2n_i}t_r\right\}, & \text{if } t_r < t_b^m \\ 2\left(\frac{1}{k_i} + \sum_{j\in\mathcal{I}_b} f(i,j)\exp\left\{\frac{k_i}{2n_i}t_r\right\}\right) + \sum_{j\in\mathcal{I}_c} f(i,j)\exp\left\{\frac{k_i}{2n_i}t_r\right\}, & \text{if } t_r \geq t_b^m \end{cases} \tag{11}$$

Next, the probability of a topology-unchanged event given recombination anywhere on a branch can be derived by integrating the previous equation over the entire length of a branch. Here, the terms $p_{b,1}$ and $p_{b,2}$ correspond to recombination occurring on branch b during a time that falls into either of the two cases in equation 11.

$$\mathbb{P}(\text{topology-unchanged}|\mathcal{S},\mathcal{G},b) = \frac{1}{t_b^u - t_b^l}\left[\sum_{i\in\mathcal{L}_b} p_{b,1}^{(i)} + \sum_{i\in\mathcal{M}_b} p_{b,2}^{(i)}\right]$$

$$where:$$

$$p_{b,1}^{(i)} = \frac{1}{k_i}\left[d_i + 2n_i\left(\exp\left\{\frac{k_i}{2n_i}\mu_i\right\} - \exp\left\{\frac{k_i}{2n_i}\sigma_i\right\}\right)\left(\sum_{j\in\mathcal{I}_{bc}} f(i,j) + \sum_{j\in\mathcal{M}_b} f(i,j)\right)\right] \tag{12}$$

$$and:$$

$$p_{b,2}^{(i)} = \frac{1}{k_i}\left[2d_i + 2n_i\left(\exp\left\{\frac{k_i}{2n_i}\mu_i\right\} - \exp\left\{\frac{k_i}{2n_i}\sigma_i\right\}\right)\left(2\sum_{j\in\mathcal{I}_b} f(i,j) + \sum_{j\in\mathcal{I}_c} f(i,j)\right)\right]$$

Finally, by summing equation 12 across all branches on a genealogy while weighting each by its proportion of summed branch lengths, we get the probability that a recombination event falling uniformly on the genealogy will result in a topology-unchanged event.

$$\begin{aligned} \mathbb{P}(\text{topology-unchanged}|\mathcal{S},\mathcal{G}) &= \sum_{b\in\mathcal{G}} \frac{t_b^u - t_b^l}{L(\mathcal{G})} \times \mathbb{P}(\text{topology-unchanged}|\mathcal{S},\mathcal{G},b) \\ &= \frac{1}{L(\mathcal{G})}\sum_{b\in\mathcal{G}}\left[\sum_{i\in\mathcal{L}_b} p_{b,1}^{(i)} + \sum_{i\in\mathcal{M}_b} p_{b,2}^{(i)}\right] \end{aligned} \tag{13}$$

2.4.4 Waiting distance to topology-change events

A recombination event either does or does not change the topology of a genealogy, and we can therefore get the probability of a topology-change event using our topology-unchanged probability statement. As with the previous waiting distance distributions, the distance between topology-change events given a parameterized MSC model can be modeled as an exponential probability distribution. Similar to how a rate parameter was derived for the distribution of waiting distances until a recombination event (equation 7), no-change event (equation 9), or tree-change event (equation 10), a rate parameter λ_t can be calculated

from equation 13 for the probability of a topology-change event.

$$\lambda_t = L(\mathcal{G}) \times r \times (1 - \mathbb{P}(\text{topology-unchanged}|\mathcal{S}, \mathcal{G})) \quad (14)$$

Unlike the exact solution for the expected waiting distance to a tree-change, the waiting distance for a topology-change is an approximation. This is because topology-change probabilities are not guaranteed to be homogeneous across some distance of the genome between topology-change events, since intermediate tree-change events could occur (e.g., the second and third recombination events in Fig. 1). We examine this and other potential sources of bias in our validations below and in the Supplementary Materials.

3 Results

3.1 Implementation

We have implemented our solutions for waiting distance calculations under the MS-SMC in the Python package *ipcoal* (McKenzie & Eaton, 2020a). This software includes functions that accept a parameterized MSC model and initial genealogy as input and return the probabilities of different recombination event types. These probabilities can be calculated for specific branches and times, for entire branches, or for entire genealogies. Functions are also available to calculate the expected waiting distances for a genealogy embedded in an MSC model, and the likelihood of MSC model parameters given a distribution of waiting distances between tree-change or topology-change events in an ARG. Our implementation is built upon *toytree* (Eaton, 2020), *scipy* (Virtanen *et al.*, 2020), and *numpy* (Harris *et al.*, 2020), and uses jit-compilation with *numba* (Lam *et al.*, 2015). Below we use *ipcoal* v.0.5.0 to demonstrate the impact of MSC model parameters on waiting distances and to validate our solutions against expectations from coalescent simulations implemented in *msprime* (v.1.1.1) (Baumdicker *et al.*, 2022). Source code is available at https://github.com/eaton-lab/ipcoal. Jupyter notebooks demonstrating the MS-SMC calculations and with reproducible code used for validations in this study are available at https://github.com/eaton-lab/waiting-distance-code.

3.2 Demonstration

Given a parameterized MSC model and initial genealogy, the probabilities of different types of recombination outcomes can be calculated and visualized as a function of when and where recombination occurs. This is demonstrated on an imbalanced 4-tip species tree with constant effective population size and with a genealogy of seven samples embedded, including three from lineage A, two from lineage B, and one from each of lineages C and D (Fig. 4a). (See Fig. S2 for details and alternative parameterizations of this simulation.) The probabilities of no-change, tree-change, or topology-change events, given a recombination event occurring on a branch at a particular time (equations 3 and 11, respectively) are shown for three selected branches on the example genealogy (Fig. 4b-d). Note that the probability of no-change and tree-change events are inversely related and sum to 1, since one or the other must occur at any recombination event. By contrast, the probability of a topology-change event is a subset of the probability of a tree-change event; it is a tree-change event where the detached branch re-coalesces with a branch other than itself, its sibling, or its parent.

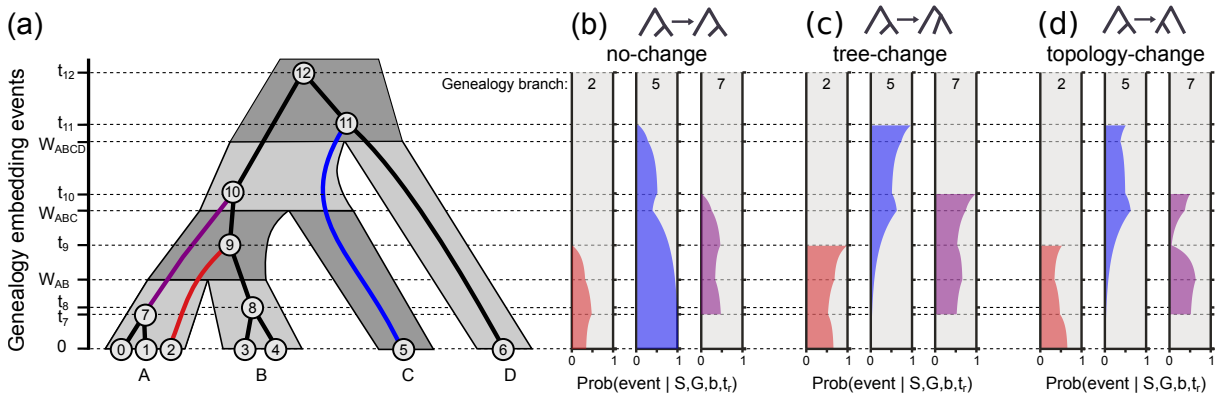

Figure 4. The MS-SMC is a model of the probability of different categorical event outcomes given recombination occurring uniformly on a genealogy embedded in a parameterized MSC model (a). A recombination event can cause one of three possible recombination event types between two sequential genealogies in a genome: *no-change*, *tree-change*, or *topology-change*. The probability of these event types are calculated by integrating over each branch on the genealogy on which recombination can occur; which in turn is calculated by integrating over each position on a genealogy branch at which recombination can occur. (b-d) The probability that a recombination event causes a no-change, tree-change, or topology-change event, for the example genealogy embedded in a species tree, was calculated for three selected genealogy branches (2: red; 5: blue; and 7: purple), at each position along the branch where recombination could occur.

In general, the probability of a no-change event decreases, and the probability of a tree-change event increases, as recombination occurs closer to the top of a genealogy branch (further back in time). This makes intuitive sense, since when recombination occurs at the top of a branch there is less time for it to re-coalesce with its same branch. Although this is a general trend, these probabilities do not behave monotonically with respect to time as they would in a single-population model with constant N_e (Deng *et al.*, 2021). Instead, probabilities increase or decrease through the length of each interval as a function of the rates of coalescence in subsequent intervals and the probability that a detached lineage will re-coalesce in one of those intervals.

For example, consider genealogy branch 2, which exhibits an increase in the probability of no-change through its first branch interval from time 0 to t_7 but then a decrease through the next interval from t_7 to W_{AB} (Fig. 4b). The observed increase through the first interval is influenced by the fact that a re-coalescence in the subsequent interval is more likely to cause a no-change event, since that interval contains only two samples instead of three. By contrast, within the second interval, recombination events near the top are approaching the next species tree divergence event. After that event, the number of samples will increase back from 2 to 3, thus decreasing the probability of a no-change event. This visualization demonstrates how the probabilities of different recombination event types represent an integration over all the positions on a branch where recombination could occur, and all positions at or above each of these points (whether on the same or different available branches) where a detached subtree could re-coalesce.

Genealogy branch 7 provides a clear example for examining the probabilities of tree- and topology-change events. Of particular interest is the interval from W_{AB} to W_{ABC} where these probabilities diverge significantly (Fig. 4c-d). The probability of topology-change decreases faster than the probability of tree-

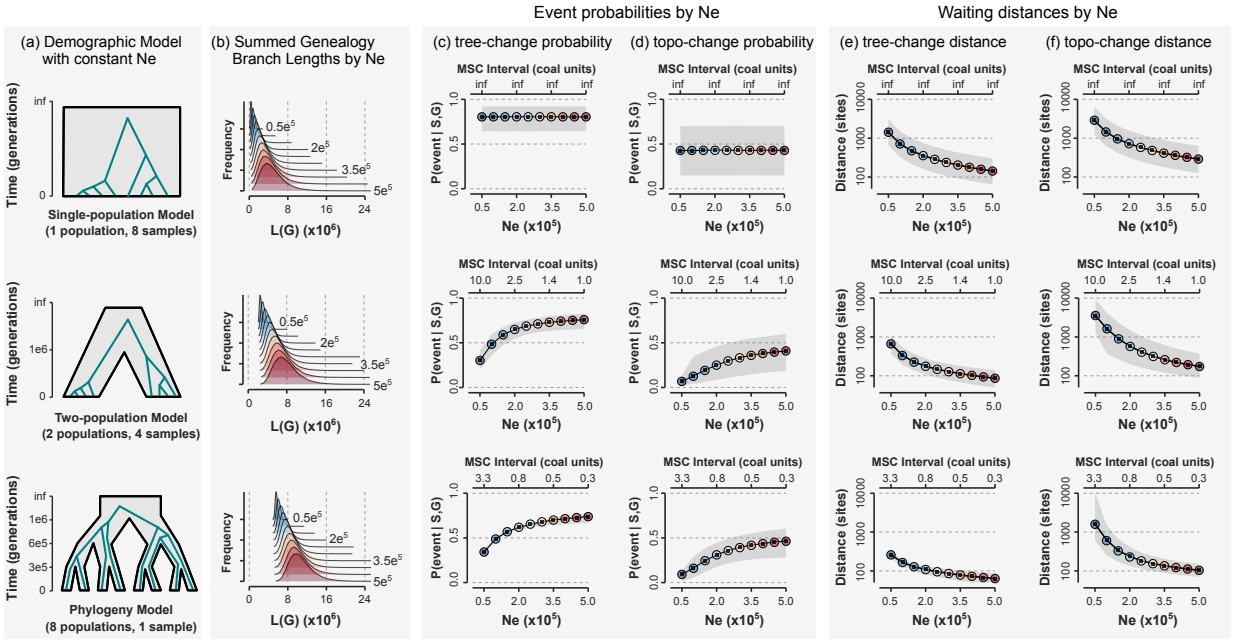

Figure 5. MS-SMC predictions validated against coalescent simulations. (a) Results are shown for three models containing 1, 2, or 8 populations. For each model, 100K tree sequences were simulated for 10 different constant N_e values between 50K and 500K. (b) The distributions of summed edge lengths of the first genealogy in each tree sequence. (c-d) The mean frequency (black square) with which the first observed recombination event was a tree-change (c) or topology-change (d) in a simulated tree sequence, and the mean (colored circle) and 95% CI (grey fill) of the predicted probability of tree or topology-change calculated from the first embedded genealogy in each tree sequence. Probabilities are constant with respect to N_e in the single population model but vary in models with population structure (also shown with respect to species tree interval lengths in coalescent units, across the top axis). (e-f) The mean waiting distance (black square) until the first observed tree-change (e) or topology-change (f) in a simulated tree sequence, and the mean (colored circle) and 95% CI (grey fill) of predicted waiting distances calculated using the first embedded genealogy in each tree sequence.

change as recombination occurs closer to node t_9. This is because following t_9 there is a large stretch of time during which re-coalescence can only occur with the same branch or its sibling, neither of which can cause a topology-change event. It is only after W_{ABC} that it is once again possible for re-coalescence to occur with a more distant branch that would result in topology-change. If the effective population size of this species tree interval (AB) were greater, then the probability of re-coalescence in a deeper interval would be more likely, and the probability of topology-change would decrease less severely near t_9. This is true more generally, as can be seen by comparing edge probabilities across MSC models with different effective population sizes (Fig. S2). Effective population size affects the rate of re-coalescence and thus either smooths probabilities across intervals when N_e is high or accentuates differences among intervals when N_e is low.

3.3 Validation

To validate our analytical solutions for the probabilities of different recombination event outcomes and their associated waiting distances, we compared predictions of the MS-SMC with results from stochastic coalescent simulations. We set up three scenarios with increasing amounts of population structure: a single-population model, a two-population model, and an 8-tip phylogeny model (Fig. 5a). All analyses used a constant per-site per-generation recombination rate of 2e-9 and simulated tree sequences using the coalescent with recombination (i.e., the "hudson" ancestry model in msprime as opposed to the "smc_prime" model, which is an approximation), and the argument "record_full_arg=True" (to retain records of invisible recombination events). For each model we simulated genealogies for the same total number of samples (8, unless specified), divided evenly among lineages when models include multiple populations (Fig. 5a).

The exponential rate parameter (λ) for a probability distribution of waiting distances is a product of the per-site per-generation recombination rate (r), the sum of edge lengths on the current genealogy ($L(\mathcal{G})$), and the probability ($\mathbb{P}$) of the specified event type (equations 9, 10, and 14). Across the three models examined, r remains constant, but both $L(\mathcal{G})$ and $\mathbb{P}$ can vary due to population structure, where the effect of structure is scaled by N_e. Therefore, we examined $L(\mathcal{G})$, $\mathbb{P}$, and the expected waiting distance calculated from their product, for each demographic model across a range of N_e values (50K – 500K; Fig. 5b-f). At each value of N_e we simulated 100K tree sequences for each demographic model.

Each simulated tree sequence contains a series of trees and intervals representing stochastic outcomes of the coalescent with recombination. Over many replicates, we expect the mean waiting distances until the first tree and topology-change events in simulations to match the predicted waiting distances estimated under the MS-SMC, computed from only observing the starting tree in each tree sequence. (Note that to avoid any potential bias associated with the first tree interval in simulated tree sequences we actually advanced to the first tree after the first topology-change event to serve as the starting tree in all analyses.) To measure tree and topology-change waiting distances in tree sequences we recorded the sum length of the interval that includes the starting tree, and any subsequent intervals in which no tree-change occurred, or no topology-change occurred, respectively. To measure the probability of each event type in simulations we recorded which event type (including no-change events) was the first to occur after the starting tree in each tree sequence. The MS-SMC probabilities of each event type were computed in *ipcoal* by embedding the starting tree of each tree sequence into the parameterized MSC model. Expected waiting distances under the MS-SMC were computed as 1 over the product of the event probabilities, r, and $L(\mathcal{G})$ of the starting tree.

Population structure enforces a limit on the minimum length of coalescent times by requiring that genealogies can be embedded in a species tree. This has the effect of shifting both the minimum and mean of $L(\mathcal{G})$ higher across all values of N_e (Fig. 5b). Because the per-generation recombination rate interacts with $L(\mathcal{G})$ (the opportunity over which recombination can occur) to determine the frequency of recombination, larger $L(\mathcal{G})$ induced by population structure will tend to decrease waiting distances between recombination events, all else being equal. However, all else does not remain equal. Instead, population structure in MSC models has a simultaneous opposing effect of increasing the mean waiting distance to tree or topology change events by affecting the event probabilities (Fig. 5c-d). This is most clear at low values of N_e, where shorter coalescent times are less likely to span the barriers between lineages in an MSC model. This has

the effect of increasing the probability of no-change events relative to tree or topology-change events. By contrast, when N_e is high the barriers in an MSC model have little effect on coalescence probabilities, and the tree and topology-change event probabilities in MSC models converge towards those seen in the single population model (Fig. 5c-d). This highlights the relationship between MSC model parameters and the waiting distances between different recombination event types. In MSC models, waiting distances to the three different recombination event types can vary as a consequence of the model parameters' effects on $L(\mathcal{G})$ and $\mathbb{P}$, whereas in a single population model each waiting distance is simply scaled by $L(\mathcal{G})$.

Our analytical predictions under the MS-SMC converge accurately on the mean results from stochastic coalescent simulations (Fig. 5c-f). Moreover, by examining the variance in these predictions with respect to MSC model parameters we further gain insights into the information contained in spatial genealogical patterns. For example, in the single population model there is high variance in both the probabilities of tree and topology changes, as well as in genealogy lengths, at any given N_e value. Consequently, waiting distances also exhibit high variance. Although waiting distances correlate with population N_e in this model, the differences in mean waiting distances are small relative to the variance. By contrast, multispecies models exhibit much less variance in predicted probabilities of tree or topology changes given a set of MSC model parameters (Fig. 5c-d) and also exhibit less variation in genealogy lengths. This leads to a stronger relationship between MSC model parameters and expected waiting distances (Fig. 5e-f), such that models with different parameters have less overlap in waiting distance expectations. Overall, this demonstrates that estimations of tree- and topology-change waiting distances calculated under the MS-SMC are accurate, and contain information for inferring population demographic parameters.

3.4 Bias in waiting distance estimation

Estimated waiting distances under the MS-SMC harbor two potential sources of bias, the first stemming from assumptions of the SMC' approximation, and the second from the approximate nature of waiting distance estimation for topology-change events. We examined both of these sources of error through comparison to stochastic simulations and found that their effects are generally small, and that multispecies models exhibit a similar magnitude of error as single population coalescent models (see "Investigating bias" section in Supplementary Materials; Fig. S3, Fig. S4, Fig. S5). The SMC' approximation introduces very little bias to MS-SMC estimates of tree-change waiting distances across all scenarios examined, and only significantly biases topology-change waiting distance estimates in the "species tree" demographic model scenario at very low N_e values – a scenario where genealogical discordance becomes very unlikely. This scenario is also most affected by the other source of bias, as it exhibits greatest variance in genealogy branch lengths among intervals between topology-change events. For both sources of bias, we show that error is greatly reduced by simply increasing the number of genomes sampled per lineage.

3.5 A Likelihood-based Framework for Evaluating Waiting Distances

The MS-SMC is a statistical model of the waiting distances between different types of genealogy changes in an ARG, given a parameterized MSC model. Since waiting distances between recombination events follow an exponential distribution, we can use the exponential probability density (equation 8) as the likelihood function to assess observed (or estimated) waiting distances in an ARG, by modeling the probability

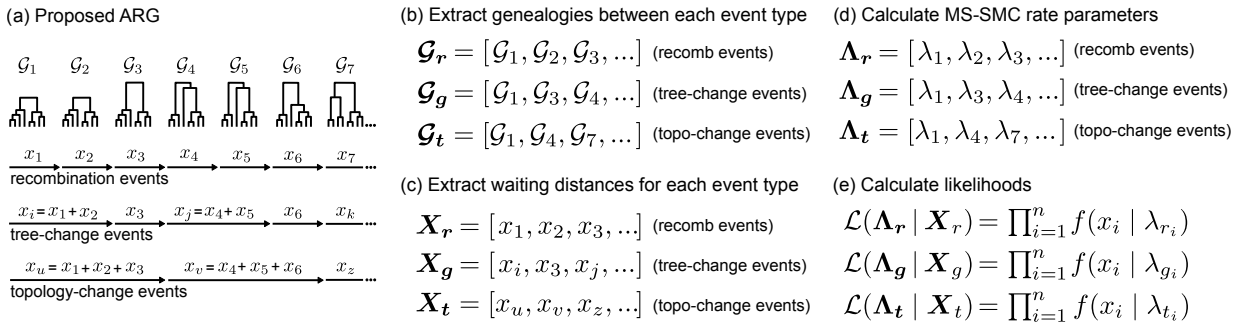

Figure 6. A likelihood framework for fitting MSC model parameters from waiting distances between categorical types of recombination events in an ARG. (a) An ARG represents a sequence of genealogies ($\mathcal{G}$) and their interval lengths (x) over a genomic region. Intervals can be delimited by all recombination events, or by a subset representing only tree-change, or only topology-change events. (b) The set of genealogies ($\boldsymbol{\mathcal{G}}$) occurring between each event type can be extracted, and similarly, (c) the set of associated interval lengths ($\boldsymbol{X}$) between each event type can be extracted. (d) A set of exponential rate parameters ($\boldsymbol{\Lambda}$) can then be estimated under the MS-SMC for the waiting distance until each type of recombination event, for each genealogy, given its embedding in a parameterized MSC model ($\mathcal{S}$) and the recombination rate (r). (e) Using the exponential probability density function, the likelihood of the MSC model parameters is calculated as the product of the probability densities for each waiting distance in $\boldsymbol{X}$, evaluated using the corresponding rate parameters in $\boldsymbol{\Lambda}$.

of these waiting distances as a function of demographic model parameters. We propose that applications of this approach can provide improvements to ARG and demographic model inference methods. Below, we describe and demonstrate one such application.

Given one or more ARGs each composing a sequence of genealogies and their interval lengths in a genome, a subset of genealogies and intervals can be extracted that represent the combined intervals between a specific type of event (Fig. 6a). For example, $\boldsymbol{\mathcal{G}_g} = (\mathcal{G}_1, \mathcal{G}_j, ...)$ can represent the subset of genealogies that occur between tree-change events and $\boldsymbol{X_g} = (\sum_{i=1}^{j} x_i, \sum_{i=j}^{k} x_i, ...,)$ the summed lengths of intervals between tree-change events (Fig. 6b-c). The same can be done for topology-change events. Given a parameterized MSC model and recombination rate we can then obtain a set of exponential rate parameters $\boldsymbol{\Lambda_g} = (\lambda_1, \lambda_j, ...)$ for the waiting distance until the next tree-change for each genealogy in $\boldsymbol{\mathcal{G}_g}$ (equation 10; Fig. 6d). Finally, using the exponential probability density function, the likelihood of the MSC model parameters is calculated as the product of the probability densities for each waiting distance in $\boldsymbol{X_g}$, evaluated using the corresponding rate parameters in $\boldsymbol{\Lambda_g}$ (Fig. 6e). Maximum likelihood optimization of the model parameters can be achieved by identifying the set of parameters – affecting $\boldsymbol{\Lambda_g}$ – that maximize the likelihood function, which quantifies the probability of the observed data given the model.

We implemented this approach to evaluate MSC model parameters using waiting distances in an ARG simulated under a two-population MSC model with variable N_e (N_e0=200K, N_e1=300K, and N_e2=400K), a divergence time W=1M generations, and recombination rate r=2e-9. We sampled four genomes per population, and simulated 50 independent tree sequences each 400Kb in length (20Mb total) under the full coalescent with recombination model. This yielded 235,872 intervals between recombination events (mean +/- S.D. length = 84.79 +/- 92.90), composing 160,501 intervals between tree-change events (mean +/- S.D. length = 124.56 +/- 135.68), and 59,288 intervals between topology-change events (mean +/- S.D.

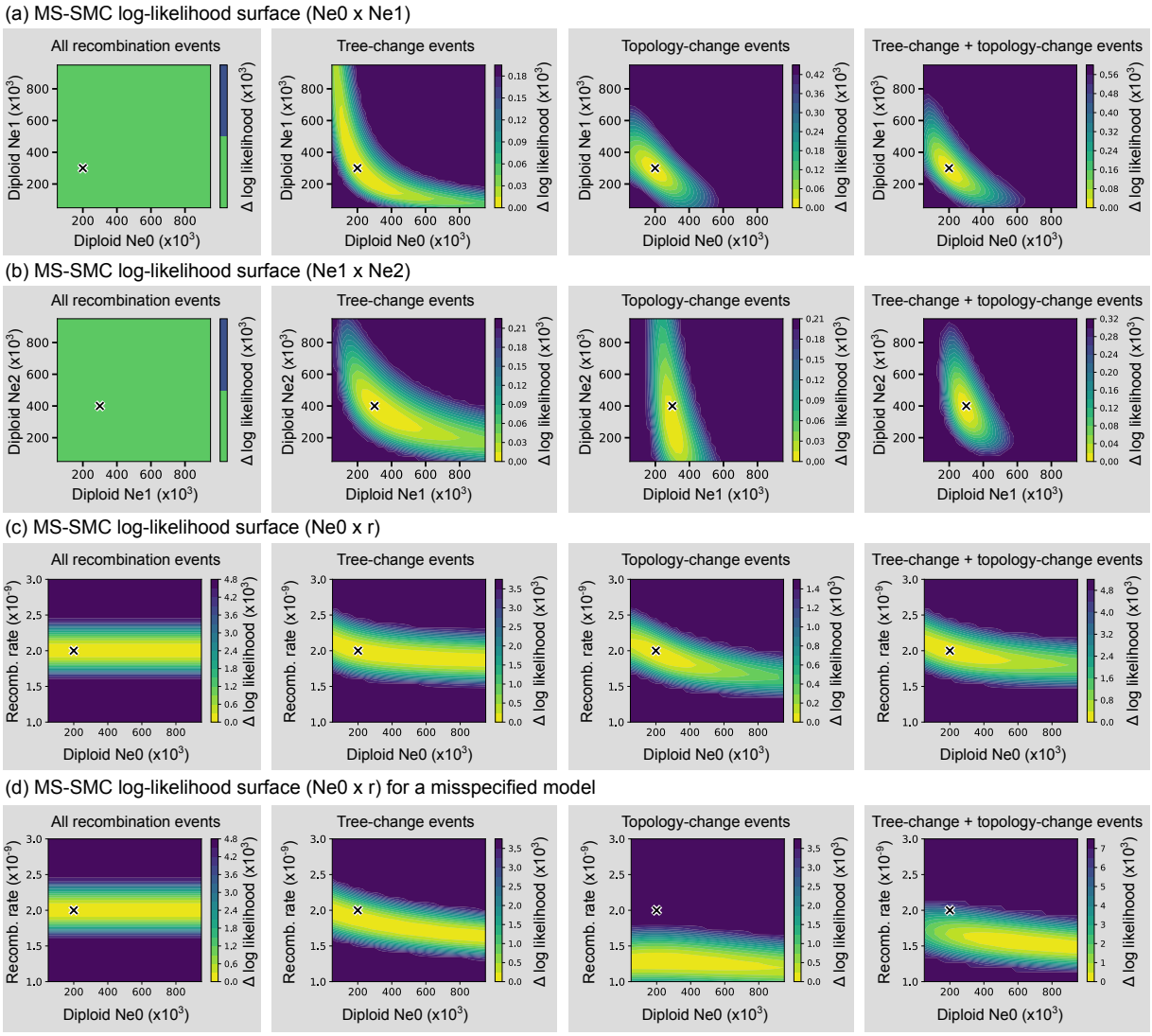

Figure 7. Implementation of a likelihood framework for fitting MSC model parameters to waiting distances in an ARG. Tree sequences were simulated under a 2-population demographic model with four MSC parameters (N_e0=200K, N_e1=300K, N_e2=400K, W=1M) and recombination rate r=2 x 10^{-9}. Log-likelihood surfaces are shown for two parameters at a time while fixing other parameters to their true value. True values are marked by an X. (a-c) Waiting distances between all recombination events provide no information for estimating MSC parameters, but the waiting distances between tree-change and topology-change events are informative about MSC parameters, both individually and in combination. (d) When waiting distances derived from a 2-population model are used to fit parameters in a single-population model they provide poor estimates of MSC parameters.

length = 336.93 +/- 441.72). To examine the information contained in different waiting distance data sets we visualized 2D log-likelihood surfaces over a grid of values for pairs of MSC model parameters, while keeping all other parameters fixed at their true values.

We compared log-likelihood surfaces for four different sources of waiting distance information, comprising the waiting distances between all recombination events, between only tree-change events, between only topology-change events, and for the combined log-likelihoods from both tree-change and topology-change waiting distances. (Fig. 6e). Note that combining tree-change and topology-change likelihoods may seem like double-counting of information, since topology-change events are a subset of the events that compose a tree-change event, in our terminology. However, our equation for the probability of a topology-change event is conditional only on $\mathcal{S}$ and $\mathcal{G}$, and not on the probability of one or more tree-change events. In addition, it is clear conceptually that these two types of event probabilities have different relationships with a species tree. As an example, consider a genealogy that has two genomes sampled per species, and is embedded in a species tree with very low N_e such that ILS is nearly impossible. The probability of a topology-change event approaches zero in this scenario, whereas the probability of a tree-change event is much less affected by species tree barriers, since this event type can still occur within each species tree interval as a change in coalescent times. We demonstrate below how the likelihood of a demographic model can be more robustly assessed by jointly incorporating both types of waiting distance observations into the likelihood calculation.

The log-likelihood surfaces show that waiting distance information in an ARG is informative for estimating MSC model parameters when analyzed under our MS-SMC model framework (Fig. 7). The waiting distances between all recombination events, which do not take into account the event type, provide no information for estimating MSC model parameters. By contrast, tree-change and topology-change waiting distances exhibit distinct ridges or peaks near the true parameter values (Fig. 7a-c). A ridge in the likelihood surface suggests some uncertainty and potential correlation structure. However, the rounder surface with more distinct peaks, seen in the combined likelihood surface from both tree-change and topology-change waiting distances, exhibits less uncertainty and correlation, suggesting the combined information from multiple waiting distance types provides the most accurate inference (Fig. 7a-c). We also used the same ARGs, simulated under a two-population model with five parameters, to examine the likelihood surface under an incorrect demographic model, based on a single population model with two parameters (Fig. 7d). Here, the waiting distance data are a poor fit to the model, providing inaccurate estimates of model parameters, especially from topology-change waiting distances. This suggests that topology-change waiting distances may be particularly informative for model selection between demographic models, such as comparing species tree topologies.

Building on the high accuracy of our MS-SMC model, as suggested by the likelihood surfaces, we proceeded to fit a full MSC model by jointly estimating all four MSC model parameters and the recombination rate from waiting distance data. We applied a Bayesian approach using the Metropolis-Hastings Markov chain Monte Carlo (MCMC) algorithm to obtain the joint posterior probability distribution of all parameters. For this, we set uninformative uniform priors on each parameter, using U(1e5, 1e6) for N_e parameters, U(1e5, 2e6) for W, and U(1e-9, 3e-9) for r. Four separate MCMC chains were each initiated from different random seeds, and each run on the same simulated ARGs from above, using the combined likelihood of both tree-change and topology-change waiting distances. The first 500 iterations were ex-

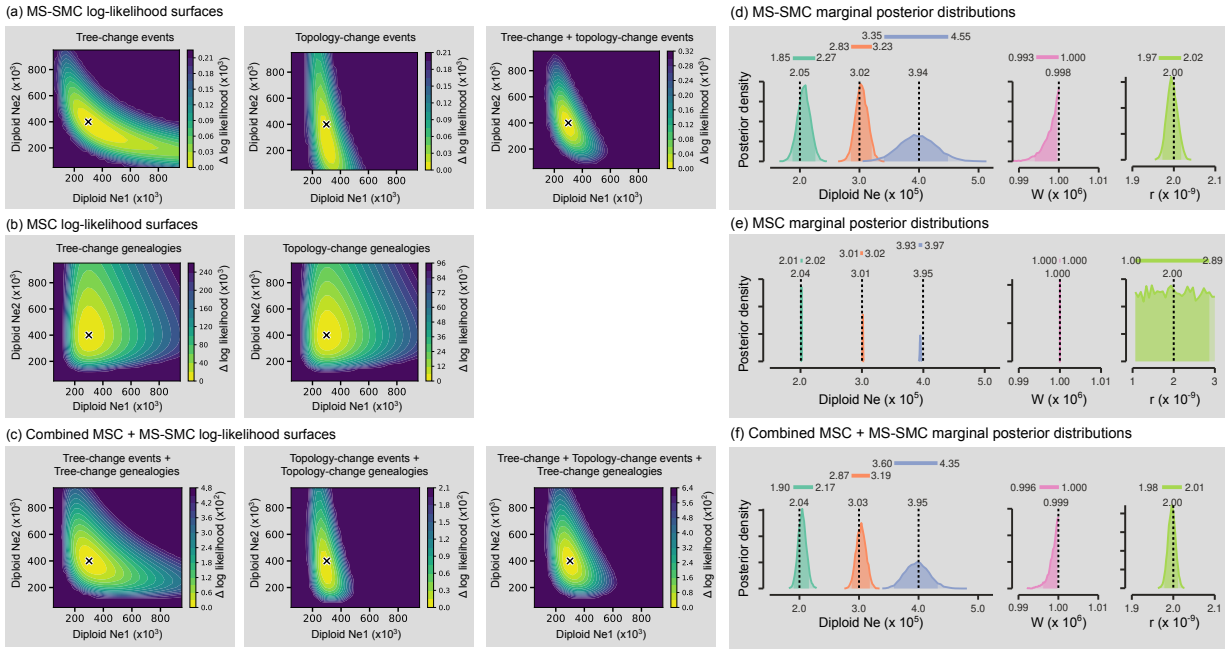

Figure 8. A comparison of likelihood-based model inference under the MS-SMC versus MSC models – i.e., when analyzing the waiting distances of genealogies versus the coalescent times in genealogies, respectively. (a-c) Log-likelihood surfaces for parameters N_e1 and N_e2 based on (a) waiting distance likelihoods computed under the MS-SMC; (b) genealogy likelihoods computed under the MSC; or (c) the combined log-likelihoods of both types of data. Note, MSC log-likelihoods are greater than MS-SMC log-likelihoods and were down-weighted to a similar scale when combined. (d-f) The marginal posterior distributions of demographic model parameters N_e0, N_e1, N_e2, W, and r jointly estimated using Bayesian inference. True demographic model parameters are indicated by a dashed black line, above which the marginal posterior mean and 95% HPD interval are shown. The marginal posterior distributions correspond to model parameter inference from (d) combined tree-change and topology-change waiting distances; (e) coalescent times of genealogies between tree-change events; and (f) the combined likelihoods of the data used in the previous two analyses, equally weighted.

cluded as burn-in and used to tune the proposal mechanism to achieve approximately 60% acceptance rates. From each chain, we sampled 2,000 posterior values, sampling every 10 iterations. All parameters in each chain were assessed for convergence to confirm that ESS scores exceeded 200. The four chains were then joined into a single combined posterior.

Our Bayesian implementation of the MS-SMC model shows that demographic model parameters can be accurately estimated from waiting distance information alone. Using waiting distances simulated under a complex two-population model with variable N_e, we recovered accurate marginal posterior estimates for all three N_e parameters, as well as the divergence time and recombination rate (Fig. 8d). Note that the marginal posterior for the divergence time (W) is truncated slightly above the true value, since values above this do not allow for all genealogies to be embedded in the demographic model, and were thus rejected. This could be handled more appropriately by using more advanced priors on W. Across all parameters of the demographic model the true simulated values fall within the inferred marginal 95% highest posterior density (HPD) intervals. This demonstrates that the tree-change and topology-change waiting distances in an ARG contain sufficient information when evaluated under the MS-SMC model to jointly infer all parameters of a reasonably complex demographic model.

3.6 Combining MS-SMC and MSC likelihoods

Finally, we compared the information contained in the lengths of genealogy or topology intervals (i.e., waiting distances examined under the MS-SMC) to the information contained in the trees within those intervals (i.e., coalescent waiting times examined under the MSC). Using the same simulated ARGs from above, we computed the log-likelihood of MSC model parameters by evaluating the probabilities of only the genealogies between tree-change or topology-change events under the MSC, only the waiting distances of those genealogies under the MS-SMC, or using both log-likelihoods combined. For MSC calculations, the probability of each genealogy was weighted by the length of sequence that it spanned, as this greatly improved accuracy compared to equal weighting, and provides the same precision of ARG information to the MSC model as is provided to the MS-SMC model. For MSC calculations we did not combine the probabilities of genealogies that occur between both tree-change and topology-change events, as this would represent double-counting of the same exact trees.

The log-likelihood surface of N_e parameters computed under the MSC model was less tightly concentrated near the true values than under the MS-SMC model, but exhibited a more round shape, suggesting less uncertainty and minimal correlation between parameters (Fig. 8a-b). The log-likelihood of the true parameter values under the MSC model was approximately 12 times greater than under the MS-SMC model, reflecting that there is generally much more information in the coalescent times in a genealogy than in the interval length that it spans. Similarly, the Δlog-likelihood across the examined parameter space was approximately three orders of magnitude greater when analyzing genealogies under the MSC compared to waiting distances under the MS-SMC.

When evaluating model parameters based on multiple criteria, inference can be improved if the corresponding likelihood surfaces exhibit orthogonal or complementary structures, as we observed here between the MSC and MS-SMC likelihood surfaces. Such differences in their shapes allow each criterion to provide unique information about the parameter space, which can improve the precision and robustness of optimization, as we showed previously for combining tree- and topology-change waiting distances. Here,

we implemented a simple weighting scheme, by uniformly dividing the MSC log-likelihoods by 1000, as this visually led to an intermediate shape of the likelihood surface. The resulting combined likelihood surfaces (Fig. 8c) are more narrowly concentrated around the true values than under the MSC model alone, and generally exhibit rounder more peaked surfaces than under the MS-SMC model alone.

We next applied our Bayesian joint inference framework to estimate all five parameters using genealogy likelihoods, or combined genealogy and waiting distance likelihoods. As before, four separate MCMC chains were run on the same ARGs from different starting seeds, checked for convergence criteria, and then combined. The marginal posterior distributions inferred from genealogy likelihoods were very narrow for all parameters except r, for which the MSC model provides no information, and thus returned the prior (Fig. 8e). The true values did not fall within the 95% HPD intervals for the N_e parameters, despite the posterior means being very close to the true values. This may reflect a slight bias within our MCMC implementation, or be caused by the non-independence of genealogies being analyzed under the MSC model. Despite this, we predicted that the combined information from genealogies and waiting distances will provide a more accurate estimate of MSC parameters than from waiting distances alone, since the combined data tend to exhibit a more peaked and uncorrelated log-likelihood surface. As predicted, the marginal posterior distributions inferred from these data are more narrow and accurate than from waiting distances alone (Fig. 8f), with all true values falling within the inferred 95% HPD intervals. This confirms that the information contained in tree- and topology-change waiting distances is not redundant with the information contained in genealogy coalescent times, and that these observations can be combined to provide additional information to evaluate the fit of an observed or proposed ARG to a demographic model.

4 Discussion

Genealogical relationships vary spatially across chromosomes, reflecting a history of recombination between genome segments inherited from different ancestors. Such variation can be modeled by the sequentially Markov coalescent, which provides a generative process upon which many statistical methods have been developed (McVean & Cardin, 2005; Spence *et al.*, 2018). However, most applications of the SMC' remain highly limited with regard to the scale over which they extract information from genomes – extending forward just one recombination event at a time. By contrast, the recent development by Deng *et al.* (2021) of solutions for predicting tree- and topology-change waiting distances under the SMC' effectively adds two additional, longer-range sources of information for any position in a genome. In their model, these distances are a result of the probabilities of different phenomenological outcomes of the SMC' process given a genealogy embedded in a single population coalescent model with constant N_e. Here we extended this framework, deriving new solutions for the probabilities of tree-change and topology-change events for a genealogy embedded in any arbitrarily parameterized species tree model. While some previous studies have explored the impact of species tree parameters on linked genealogical variation, their results have been limited to few specific cases (e.g., Slatkin & Pollack, 2006). Our generalized solutions here lay a groundwork for modeling how variation in species tree parameters affects neutral expectations of genealogical heterogeneity across chromosomes.

The multi-species sequentially Markov coalescent (MS-SMC) is a predictive model for the relationship between a parameterized species tree and the length of a genomic interval over which a genealogy will

span. Within this framework, demographic model parameters determine probabilities of coalescence in species tree intervals and prevent coalescence between lineages that are separated by species divergence events. This constrains the outcomes of the SMC' process, and thus the similarity of genealogies in sequential genomic intervals. By categorizing the continuous outcomes of this constrained SMC' process into few discrete categorical outcomes, we are able to compute the probabilities of each type, corresponding to recombination events that delimit no change to the genealogy, a tree-change, or a topology-change. Using these solutions, the effect of MSC model parameters on the probability of genealogical turnover can be computed and visualized for a single genealogy (Fig. 4; Fig. S2), or for a distribution of genealogies simulated under an MSC model (Fig. 5). Using the latter approach, we demonstrated the accuracy of our solutions by showing that the mean and variance of waiting distances predicted by our model match closely to the results of stochastic coalescent simulations performed on the same demographic model under the SMC' or full coalescent with recombination.

A complex relationship exists between a parameterized MSC model, the distribution of genealogies that can arise under that model, and the spatial distances over which those genealogies are expected to span. Previously, such patterns could only be examined through stochastic simulations. For example, McKenzie & Eaton (2020b) used exhaustive simulations to examine the effect of species tree parameters on the spanning length of genealogical topologies by varying species tree length, size, and shape. While this approach is practical for estimating the *mean* linkage across a large set of sampled genealogies under a specific demographic model, it is impractical for estimating the persistence of *individual* genealogies. The analytical solutions presented here not only enable calculating and comparing the expected interval lengths that different genealogies will span given their embedding in the same species tree, but also enabled the development of a statistical framework for computing the probability of an observed waiting distance spanned by a genealogy as a function of the species tree model.

The multi-species coalescent is the foundation of modern phylogenetic methods that aim to infer a species tree as a hierarchical model within which genealogical variation can be embedded (Degnan & Rosenberg, 2009; Maddison, 1997; Maddison & Knowles, 2006). The parameters of this model can be estimated from the distribution of coalescent times in genealogies, and many methods have been developed on this framework including full likelihood based analyses of molecular sequence data (Rannala & Yang, 2003), and pseudo-likelihood or summary based methods that analyze inferred gene tree distributions (Mirarab *et al.*, 2021). Here, we demonstrated that the parameters of a species tree model can alternatively be estimated from a completely new source of information, in the form of the waiting distances between recombination events causing a tree-change or topology-change between sequential genealogies in an ARG (Fig. 8d). Examination of joint likelihood surfaces revealed that these two types of waiting distance observations provide non-redundant information that is complementary and orthogonal, such that when combined they can intersect to provide more accurate estimates of model parameters (Fig. 7a-b). Future methods development should consider how best to capitalize on the unique information contained by combining these distinct waiting distance types while making sure to avoid shared signal between them. Similarly, although the information contained in tree- and topology-change waiting distances is less than that contained in the coalescent times of the same genealogies, we showed that these two sources of data can be combined, and are also complementary and non-redundant (Fig. 8c,f). Our approach for combining MSC and MS-SMC results was heuristic (e.g., weighting the MSC log-likelihoods by 1000) to demon-

strate complementary signals, and further effort might develop a method that combines these sources of information more effectively.

Our results primarily focus on demonstrating that waiting distances contain useful information, and more work is necessary to incorporate waiting distances into broadly usable inference methods. Specifically, this should include building on our demonstrations here to construct a rigorous analytical framework for jointly analyzing tree and topology waiting distances alongside existing sources of information (e.g., coalescence times), and to further evaluate the additional value that waiting distance information brings to specific applications. We envision future methods building upon our joint framework to evaluate the fit of ARGs to a demographic model using not only the probabilities of genealogies within the ARG, but also the probabilities of the spanning distances of topological features of those genealogies. Below we describe several of these envisioned applications. ~~We envision many future applications can build upon this joint framework for evaluating the fit of ARGs to a demographic model using not only the probabilities of genealogies within the ARG, but also the probabilities of the spanning distances of topological features of those genealogies. Below we describe several of these envisioned applications.~~

4.1 The Distribution of Genealogical Variation

One potential application of the MS-SMC model is to incorporate expectations for the spanning lengths of genealogies into theoretical models of the relationship between species tree models and the distribution of genealogical variation. Consider that much of our understanding of this relationship is derived from theoretical studies of the distribution of unlinked genealogical topologies, without regard for differences in the expected spanning lengths of the topologies (Degnan & Rosenberg, 2006; Degnan & Salter, 2005). However, as we have shown here, the same genealogy may exhibit very different expected spanning lengths between topology-change events depending on the species tree model. By incorporating topology-change probabilities calculated under the MS-SMC into theoretical models of genealogical discordance, we could shift the focus from the frequency of occurrence of each genealogical topology, to the frequency of sites evolved under each topology. This would provide a new perspective on the distribution of genealogical variation, and could spur the development of new theoretical advances.

Another more practical application of the MS-SMC is to guide the selection of appropriate locus lengths to use for gene tree inference. In theory, each locus or window should correspond to a single genealogical tree or topology. However, the mean waiting distance between topology-change events in multi-species datasets is typically much shorter (e.g., 10-100 bp) than the mean locus lengths of common subgenomic markers (e.g., >300 bp; McKenzie & Eaton, 2020b), and certainly much shorter than the size of genomic sliding windows commonly employed at genome-wide analysis scales (e.g., 100 Kb; Li *et al.*, 2019). When repeated across many loci, concatenation artifacts can cause the distribution of gene trees, or their summary statistics, to deviate from expectations under the MSC – a process termed concatalescence (Gatesy & Springer, 2013). The extent to which this process will bias MSC-based inferences remains a matter of debate. Simulation studies under a range of species tree models and parameters have shown that some inference methods are more sensitive to errors caused by intra-locus recombination than others (Lanier & Knowles, 2012; Zhu *et al.*, 2022), but this has not facilitated general recommendations that can apply to all datasets and methods. Topology-change probabilities calculated under the MS-SMC provide a framework to formalize this debate around common metrics that can be computed for any species tree,

filling a theoretical gap specifically noted by Zhu *et al.* (2022).

4.2 Applications of the MS-SMC to ARG Inference

While our demonstration of the MS-SMC framework focused on inferring species trees from ARGs, its most impactful applications may lie in the inverse approach: inferring ARGs given a demographic model. ARG inference is notoriously challenging due to the vast state space of potential ARGs and the limited information contained within intervals between recombination events, which complicates the accurate reconstruction of local genealogies. However, linkage information between neighboring intervals provides a critical source of information that can be explicitly modeled to propose ARGs that are statistically consistent with an underlying evolutionary model, such as the SMC'. Nevertheless, integrating this linkage information while navigating the immense state space of possible ARGs remains a computationally demanding task. Despite these challenges, a number of powerful tools have been developed to efficiently infer ARGs and quantify uncertainty, typically through Bayesian posterior sampling methods (Brandt *et al.*, 2022; Lewanski *et al.*, 2024).

Several challenges currently limit the application and accuracy of ARG inference at deeper phylogenetic scales. One notable limitation is the assumption that samples originate from a single population, which can bias estimates when the true demographic model involves population structure, as demonstrated in our example of model misspecification (Fig. 7d). Some methods already address this limitation, such as ARGweaver-D, which allows users to specify a demographic model upon which ARGs will be conditionally sampled (Hubisz & Siepel, 2020). This approach generates ARGs with changes between sequential genealogies that are consistent with the SMC' process occurring within a structured demographic model – i.e., consistent with the MS-SMC. However, the resulting tree- and topology-change waiting distances that arise in proposed ARGs are not currently incorporated into the likelihood calculation. We propose that our new framework, which allows computing the likelihood of a species tree model from the tree-change and topology-change waiting distances in an ARG, could enhance both the accuracy and convergence of ARG inference by providing additional criteria for assessing the fit of proposed ARGs to a species tree model.

Another potential application of the MS-SMC is to reduce the problem of ARG inference from inferring a genealogy and interval length between every recombination event, to instead infer genealogies and intervals between only a subset of events, such as tree-change or topology-change events. For example, topology-change events in particular leave more detectable signatures in sequence data for identifying break points, and occur less frequently. This could particularly benefit ARG inference above the species-level, where the lengths of intervals between recombination events can become very small, even to the extent that more than one recombination event occurs between two sequential sites, which would violate assumptions of the SMC' (Rasmussen *et al.*, 2014). In these scenarios, the distance between topology-change events will always be much longer. We do not expect that delimiting ARGs on topology-change events would introduce a significant bias, since as we demonstrated in our results, the recombination rate can still be very accurately inferred under the MS-SMC from the interval lengths between tree- and/or topology-change events alone (Fig. 8d). By reducing the number of breakpoints and genealogies that must be inferred, this would effectively reduce the complexity of the ARG inference problem, which could improve the efficiency and mixing of MCMC algorithms used to sample ARGs.

4.3 Applications of the MS-SMC to Species Tree Inference

In contrast to current species tree inference methods which tend to either ignore genetic linkage, or to discard the vast majority of sequenced data in effort to avoid it, one could envision an alternative, spatially-aware phylogenetic inference framework that more effectively utilizes linked genomic data. This would mark a major transition in phylogenetics, where recombination could be viewed as a source of information rather than a source of error. We see the MS-SMC as an important step in this direction.

As a first application of the MS-SMC, we demonstrated a likelihood-based framework to fit demographic model parameters from a known ARG based on the distribution of tree-change and topology-change waiting distances. When waiting distances were simulated under one demographic model, but used to fit parameters of a different one, topology-change waiting distances were particularly informative in revealing that the incorrect model was a poor fit to the data. This suggests that the distinct tree and topology waiting distance distributions within ARGs generated under one species tree model versus another can be useful for distinguishing between models, which is an important component of species tree inference, network inference, and species delimitation. In this context, our likelihood-based framework for analyzing waiting distances could contribute to the analysis of linked genomic data not only for improving the inference of ARGs conditional on a demographic model, but also for comparing the fit of alternative demographic models. However, the most significant challenge to incorporating waiting distance information into an inference framework is the fact that ARGs, and thus the waiting distances contained within them, are not directly observable, and must instead be inferred from observed sequence variation. One solution to this problem is to evaluate demographic models by marginalizing over uncertainty in a posterior sample of ARGs; another solution is to try to bypass ARG inference altogether. We discuss each of these approaches below.

Given the inherent complexity of ARG inference, the development of a joint framework for simultaneous inference of ARGs and species trees remains a significant challenge. However, if the analysis is restricted to a small number of competing species tree hypotheses, existing ARG inference tools can already offer a powerful framework for demographic model comparison. Tools like ARGWeaver-D, for instance, not only generate posterior samples of ARGs but also calculate the likelihood of the user-defined demographic model – though note that demographic model parameters are typically first inferred separately from unlinked genomic data prior to this analysis and then fixed (Hubisz & Siepel, 2020). While this approach does not yet scale well to large demographic models of the size that are often investigated during species tree inference, it can theoretically provide additional benefits over the analysis of unlinked data, including greater power to infer accurate local genealogies by incorporating linkage information, and the ability to examine local genealogies as a byproduct. In addition, by generating ARGs as a byproduct, this would provide the ability to analyze tree- and topology-change waiting distances as additional criteria for evaluating demographic model likelihoods. In this context, our description above of the multiple potential applications of the MS-SMC to improve ARG inference conditioned on a demographic model, also represent ways in which the MS-SMC could improve methods for evaluating and comparing demographic models.

A situation where this may be particularly rewarding is in the evaluation of complex demographic models with migration, which are also often represented as phylogenetic networks. In network models, each genealogy can trace back a coalescent history through one or more paths in a model with different proba-

bilities, corresponding to an embedding of the genealogy into one species tree model or another (Degnan, 2018; Wen *et al.*, 2016). When each genealogy is analyzed individually, as in the case of unlinked genomic data, each provides little information about the network, and whether discordant genealogies correspond to introgression versus incomplete lineage sorting (ILS). Furthermore, many alternative network hypotheses are often unidentifiable based on the frequencies of gene tree patterns alone (Solís-Lemus & Ané, 2016). By contrast, ARG inference-based methods for evaluating structured demographic models with migration (Guo *et al.*, 2022; Hubisz & Siepel, 2020) have shown great power to infer demographic migration parameters and distinguish between ILS and introgression in the history of local genealogies. Given our expectation that waiting distance distributions are informative about alternative species tree models, we predict that incorporating waiting distance probabilities into local ARG inference could further improve the power of these methods to map genealogies into alternative coalescent paths through phylogenetic networks.

Finally, we envision that our framework for evaluating the likelihood of demographic models based only on the waiting distances in ARGs could serve as the basis for the development of demographic inference methods for analyzing linked genome data that do not require ARG inference. Conceptually, a method that aims to bypass ARG inference when analyzing waiting distance distributions would be similar to the implementation of SNAPP, which aims to bypass the problem of gene tree inference when inferring species trees (Bryant *et al.*, 2012). In SNAPP, this is accomplished through a Bayesian implementation for evaluating SNP patterns that integrates over the distribution of genealogies that could produce each SNP. Recent work has pointed out drawbacks of this approach when applied to pools of unlinked SNPs, since assuming independence among SNPs can lead to a loss of information (Zhu & Yang, 2021). Our vision for a theoretical ARG-based extension of SNAPP would address this concern by specifically modeling the linkage between non-independent SNPs as a source of information. For example, linked SNPs that evolve on conflicting topologies can provide information about the probability of a topology-change event occurring within the distance that separates them. Because topology-change waiting distances are inherently linked to both the genealogy and species tree, these waiting distances could contribute to evaluating species trees in the form of waiting distance likelihoods, and could also possibly feedback to improve the calculation of coalescent likelihoods, by providing information that constrains the space of possible genealogies at each SNP.

4.4 Conclusions

We derived a generalized model for the distribution of waiting distances between changes in a genealogical tree or topology, given a parameterized species tree model. Beyond its applications for species tree and ARG inference, this framework provides a foundation for establishing neutral expectation for the spatial turnover of genealogical relationships across a genome. Such expectations are particularly useful for identifying deviations caused by model violations, such as introgression, or non-neutral processes like selection. With genome-scale data now widely available, gene tree inference is commonly performed in sliding windows across a genome to examine the spatial distributions of topological relationships, where deviations of patterns from a genome-wide average are interpreted as evidence of selection or introgression (Li *et al.*, 2019; Martin & Belleghem, 2017; Zhang *et al.*, 2016). These interpretations are typically based on the lengths of genomic intervals over which particular topologies are observed, sometimes in relation

to an estimated recombination map. We suggest that such conclusions should be critically evaluated when made without reference to a null model-based expectation. Our results show that neutral expectations for waiting distances between genealogy changes can exhibit considerable variance, and that this variance is spatially auto-correlated, meaning that a clade or topology may persist over long intervals of a genome simply by chance. By providing analytical solutions for the distribution of the waiting distance to tree and topology changes under a demographic model, our results provide a new statistical framework for evaluating local genealogical patterns.

4.5 Acknowledgements

This work was supported by the National Science Foundation (NSF DEB-2046813 awarded to D.A.R.E. and NSF Graduate Research Fellowship DGE 16-44869 awarded to P.F.M.). Thanks to Yun Deng for discussion on waiting distance methods, to Jerome Kelleher for and two anonymous reviewers for suggestions that improved the manuscript, and to members of the Eaton Lab for valuable feedback.

4.6 Data Availability

Code to calculate MS-SMC probabilities and waiting distances is implemented in the Python package *ipcoal* (https://github.com/eaton-lab/ipcoal). Jupyter notebooks demonstrating the MS-SMC calculations and with reproducible code used for validations in this study are available at https://github.com/eaton-lab/waiting-distance-code. Notebooks and code were also archived in DRYAD at https://doi.org/10.5061/dryad.jdfn2z3n7 (Reviewer Sharelink: http://datadryad.org/stash/share/_4s04af8qeWaVNIzQGs0klGrMEFBhoqlWIxgu66h6WA).

References

Baum, D.A. (2007). Concordance Trees, Concordance Factors, and the Exploration of Reticulate Genealogy. *Taxon*, 56, 417–426. 4

Baumdicker, F., Bisschop, G., Goldstein, D., Gower, G., Ragsdale, A.P., Tsambos, G., Zhu, S., Eldon, B., Ellerman, E.C., Galloway, J.G., Gladstein, A.L., Gorjanc, G., Guo, B., Jeffery, B., Kretzschumar, W.W., Lohse, K., Matschiner, M., Nelson, D., Pope, N.S., Quinto-Cortés, C.D., Rodrigues, M.F., Saunack, K., Sellinger, T., Thornton, K., van Kemenade, H., Wohns, A.W., Wong, Y., Gravel, S., Kern, A.D., Koskela, J., Ralph, P.L. & Kelleher, J. (2022). Efficient ancestry and mutation simulation with msprime 1.0. *Genetics*, 220, iyab229. 11

Brandt, D., Wei, X., Deng, Y., Vaughn, A.H. & Nielsen, R. (2022). Evaluation of methods for estimating coalescence times using ancestral recombination graphs. *Genetics*, 221, iyac044. 2, 24

Bryant, D., Bouckaert, R., Felsenstein, J., Rosenberg, N.A. & RoyChoudhury, A. (2012). Inferring species trees directly from biallelic genetic markers: bypassing gene trees in a full coalescent analysis. *Molecular biology and evolution*, 29, 1917–1932. 26

Degnan, J.H. (2018). Modeling hybridization under the network multispecies coalescent. *Systematic biology*, 67, 786–799. 26

Degnan, J.H. & Rosenberg, N.A. (2006). Discordance of species trees with their most likely gene trees. *PLOS Genetics*, 2, 1–7. 23

Degnan, J.H. & Rosenberg, N.A. (2009). Gene tree discordance, phylogenetic inference and the multispecies coalescent. *Trends in ecology & evolution*, 24, 332–340. 1, 4, 22

Degnan, J.H. & Salter, L.A. (2005). Gene tree distributions under the coalescent process. *Evolution*, 59, 24–37. 23

Deng, Y., Song, Y.S. & Nielsen, R. (2021). The distribution of waiting distances in ancestral recombination graphs. *Theoretical Population Biology*, 141, 34–43. 3, 4, 9, 12, 21, 40, 41, 45

Eaton, D.A.R. (2020). Toytree: A minimalist tree visualization and manipulation library for Python. *Methods in Ecology and Evolution*, 11, 187–191. 11

Gatesy, J. & Springer, M.S. (2013). Concatenation versus coalescence versus "concatalescence". *Proceedings of the National Academy of Sciences*, 110, E1179–E1179. Publisher: Proceedings of the National Academy of Sciences. 23

Griffiths, R. & Marjoram, P. (1996). An ancestral recombination graph. In: *Progress in population genetics and human evolution*. Springer-Verlag, Berlin, pp. 257–270. 2

Guo, F., Carbone, I. & Rasmussen, D.A. (2022). Recombination-aware phylogeographic inference using the structured coalescent with ancestral recombination. *PLoS Computational Biology*, 18, e1010422. 26

Harris, C.R., Millman, K.J., van der Walt, S.J., Gommers, R., Virtanen, P., Cournapeau, D., Wieser, E., Taylor, J., Berg, S., Smith, N.J., Kern, R., Picus, M., Hoyer, S., van Kerkwijk, M.H., Brett, M., Haldane, A., del Río, J.F., Wiebe, M., Peterson, P., Gérard-Marchant, P., Sheppard, K., Reddy, T., Weckesser, W., Abbasi, H., Gohlke, C. & Oliphant, T.E. (2020). Array programming with NumPy. *Nature*, 585, 357–362. 11

Hubisz, M. & Siepel, A. (2020). Inference of ancestral recombination graphs using argweaver. In: *Statistical Population Genomics*. Humana, New York, NY, pp. 231–266. 2, 24, 25, 26

Hudson, R.R. (1983). Properties of a neutral allele model with intragenic recombination. *Theoretical population biology*, 23, 183–201. 2

Kelleher, J., Etheridge, A.M. & McVean, G. (2016). Efficient coalescent simulation and genealogical analysis for large sample sizes. *PLoS computational biology*, 12, e1004842. 2

Kingman, J.F.C. (1982). The coalescent. *Stochastic processes and their applications*, 13, 235–248. 1, 4, 5

Knowles, L.L. & Kubatko, L.S. (2011). *Estimating Species Trees: Practical and Theoretical Aspects*. John Wiley and Sons. 4

Lam, S.K., Pitrou, A. & Seibert, S. (2015). Numba: A llvm-based python jit compiler. In: *Proceedings of the Second Workshop on the LLVM Compiler Infrastructure in HPC*. pp. 1–6. 11

Lanier, H.C. & Knowles, L.L. (2012). Is Recombination a Problem for Species-Tree Analyses? *Systematic Biology*, 61, 691–701. 23

Lewanski, A.L., Grundler, M.C. & Bradburd, G.S. (2024). The era of the ARG: An introduction to ancestral recombination graphs and their significance in empirical evolutionary genomics. *PLOS Genetics*, 20, e1011110. Publisher: Public Library of Science. 24

Li, G., Figueiró, H.V., Eizirik, E. & Murphy, W.J. (2019). Recombination-aware phylogenomics reveals the structured genomic landscape of hybridizing cat species. *Molecular biology and evolution*, 36, 2111–2126. 23, 26

Li, H. & Durbin, R. (2011). Inference of human population history from individual whole-genome sequences. *Nature*, 475, 493–496. 2

Maddison, W.P. (1997). Gene trees in species trees. *Systematic biology*, 46, 523–536. 1, 22

Maddison, W.P. & Knowles, L.L. (2006). Inferring phylogeny despite incomplete lineage sorting. *Systematic biology*, 55, 21–30. 1, 22

Marjoram, P. & Wall, J.D. (2006). Fast" coalescent" simulation. *BMC genetics*, 7, 1–9. 2

Martin, S.H. & Belleghem, S.M.V. (2017). Exploring Evolutionary Relationships Across the Genome Using Topology Weighting. *Genetics*, 206, 429–438. 26

McKenzie, P.F. & Eaton, D.A.R. (2020a). ipcoal: an interactive Python package for simulating and analyzing genealogies and sequences on a species tree or network. *Bioinformatics*. 11

McKenzie, P.F. & Eaton, D.A.R. (2020b). The Multispecies Coalescent in Space and Time. *bioRxiv*, p. 2020.08.02.233395. 22, 23

McVean, G.A. & Cardin, N.J. (2005). Approximating the coalescent with recombination. *Philosophical Transactions of the Royal Society B: Biological Sciences*, 360, 1387–1393. 2, 21

Mirarab, S., Nakhleh, L. & Warnow, T. (2021). Multispecies Coalescent: Theory and Applications in Phylogenetics. *Annual Review of Ecology, Evolution, and Systematics*, 52, 247–268. Publisher: Annual Reviews. 22

Rannala, B. & Yang, Z. (2003). Bayes estimation of species divergence times and ancestral population sizes using dna sequences from multiple loci. *Genetics*, 164, 1645–1656. 2, 5, 22

Rasmussen, M.D., Hubisz, M.J., Gronau, I. & Siepel, A. (2014). Genome-wide inference of ancestral recombination graphs. *PLoS genetics*, 10, e1004342. 2, 24

Schiffels, S. & Durbin, R. (2014). Inferring human population size and separation history from multiple genome sequences. *Nature Genetics*, 46, 919–925. Number: 8 Publisher: Nature Publishing Group. 2

Slatkin, M. & Pollack, J.L. (2006). The concordance of gene trees and species trees at two linked loci. *Genetics*, 172, 1979–1984. 21

Solís-Lemus, C. & Ané, C. (2016). Inferring Phylogenetic Networks with Maximum Pseudolikelihood under Incomplete Lineage Sorting. *PLOS Genetics*, 12, e1005896. Publisher: Public Library of Science. 26

Spence, J.P., Steinrücken, M., Terhorst, J. & Song, Y.S. (2018). Inference of population history using coalescent HMMs: review and outlook. *Current Opinion in Genetics & Development*, 53, 70–76. 2, 21

Virtanen, P., Gommers, R., Oliphant, T.E., Haberland, M., Reddy, T., Cournapeau, D., Burovski, E., Peterson, P., Weckesser, W., Bright, J., van der Walt, S.J., Brett, M., Wilson, J., Millman, K.J., Mayorov, N., Nelson, A.R.J., Jones, E., Kern, R., Larson, E., Carey, C.J., Polat, İ., Feng, Y., Moore, E.W., VanderPlas, J., Laxalde, D., Perktold, J., Cimrman, R., Henriksen, I., Quintero, E.A., Harris, C.R., Archibald, A.M., Ribeiro, A.H., Pedregosa, F., van Mulbregt, P. & SciPy 1.0 Contributors (2020). SciPy 1.0: Fundamental Algorithms for Scientific Computing in Python. *Nature Methods*, 17, 261–272. 11

Wen, D., Yu, Y. & Nakhleh, L. (2016). Bayesian Inference of Reticulate Phylogenies under the Multispecies Network Coalescent. *PLOS Genetics*, 12, e1006006. Publisher: Public Library of Science. 26

Wilton, P.R., Carmi, S. & Hobolth, A. (2015). The smc' is a highly accurate approximation to the ancestral recombination graph. *Genetics*, 200, 343–355. 3, 4

Wiuf, C. & Hein, J. (1999a). The Ancestry of a Sample of Sequences Subject to Recombination. *Genetics*, 151, 1217–1228. 8

Wiuf, C. & Hein, J. (1999b). Recombination as a Point Process along Sequences. *Theoretical Population Biology*, 55, 248–259. 2

Zhang, W., Dasmahapatra, K.K., Mallet, J., Moreira, G.R. & Kronforst, M.R. (2016). Genome-wide introgression among distantly related heliconius butterfly species. *Genome biology*, 17, 1–15. 26

Zhu, T., Flouri, T. & Yang, Z. (2022). A simulation study to examine the impact of recombination on phylogenomic inferences under the multispecies coalescent model. *Molecular Ecology*, 31, 2814–2829. 23, 24

Zhu, T. & Yang, Z. (2021). Complexity of the simplest species tree problem. *Molecular Biology and Evolution*, 38, 3993–4009. 26

5 Supplementary Information

5.1 Supplementary Figures

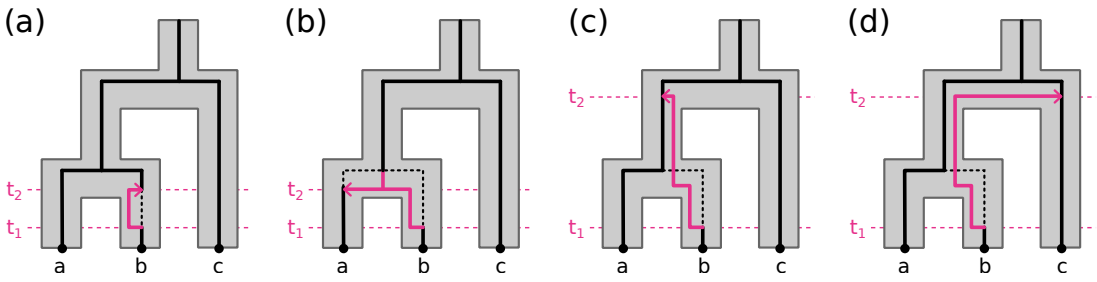

Figure S1. Four categories of outcomes from a recombination event occurring on a genealogy at time t_1, dictated by random subtree re-coalescence with a remaining lineage under the SMC' process at time t_2. (a) The detached subtree re-coalesces with the original lineage from which it was detached, leading to no change between the starting genealogy and subsequent genealogy. (b) The detached subtree re-coalesces with its sibling lineage prior to their previous coalescence, leading to a shortening of their coalescence time. (c) The detached subtree re-coalesces with its parent lineage, leading to a lengthening of the coalescent time between the detached subtree lineage and its sibling lineage. (d) The detached subtree re-coalesces with a lineage other than itself, its sibling, or its parent lineage, leading to a topology-change.

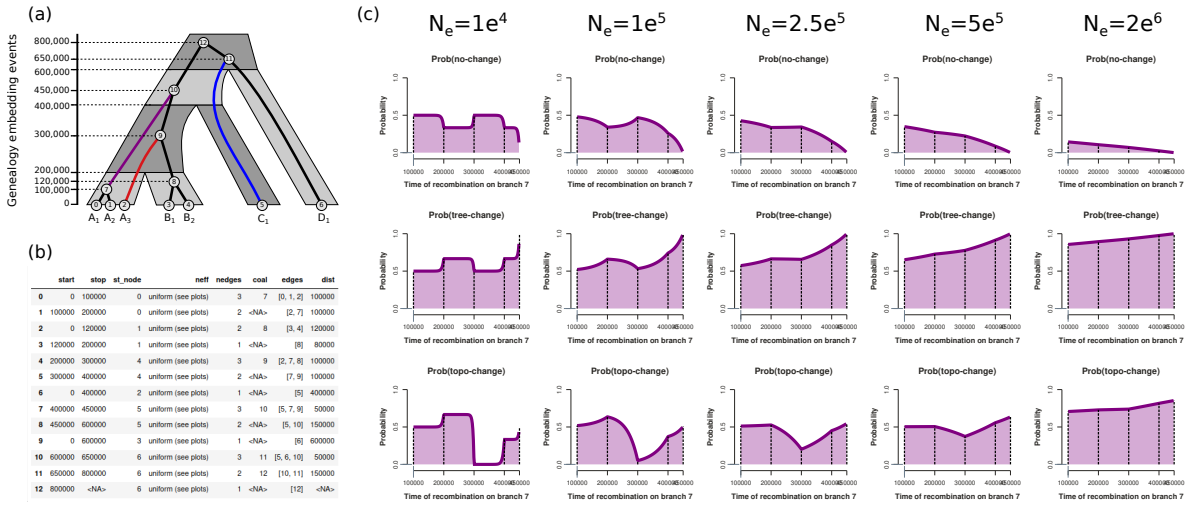

	start	stop	st_node		neff	nedges	coal	edges	dist
0	0	100000	0	uniform (see plots)	3	7	[0, 1, 2]	100000
1	100000	200000	0	uniform (see plots)	2	<NA>	[2, 7]	100000
2	0	120000	1	uniform (see plots)	2	8	[3, 4]	120000
3	120000	200000	1	uniform (see plots)	1	<NA>	[8]	80000
4	200000	300000	4	uniform (see plots)	3	9	[2, 7, 8]	100000
5	300000	400000	4	uniform (see plots)	2	<NA>	[7, 9]	100000
6	0	400000	2	uniform (see plots)	1	<NA>	[5]	400000
7	400000	450000	5	uniform (see plots)	3	10	[5, 7, 9]	50000
8	450000	600000	5	uniform (see plots)	2	<NA>	[5, 10]	150000
9	0	600000	3	uniform (see plots)	1	<NA>	[6]	600000
10	600000	650000	6	uniform (see plots)	3	11	[5, 6, 10]	50000
11	650000	800000	6	uniform (see plots)	2	12	[10, 11]	150000
12	800000	<NA>	6	uniform (see plots)	1	<NA>	[12]	<NA>

Figure S2. Probabilities of different recombination event outcomes for a selected genealogy edge as a function of the time at which recombination occurs and of the constant effective population size. (a) An MSC model with edge lengths in units of generations and an example genealogy embedded. (b) An genealogy embedding table for the example MSC model and genealogy. (c) Probabilities of different recombination event outcomes across genealogy edge 7. When N_e is low, probabilities are nearly constant with respect to time within each interval since re-coalescence in later intervals is unlikely. When N_e is high, probabilities change nearly monotonically across the length of an edge since population structure does little to constrain the time of re-coalescence.

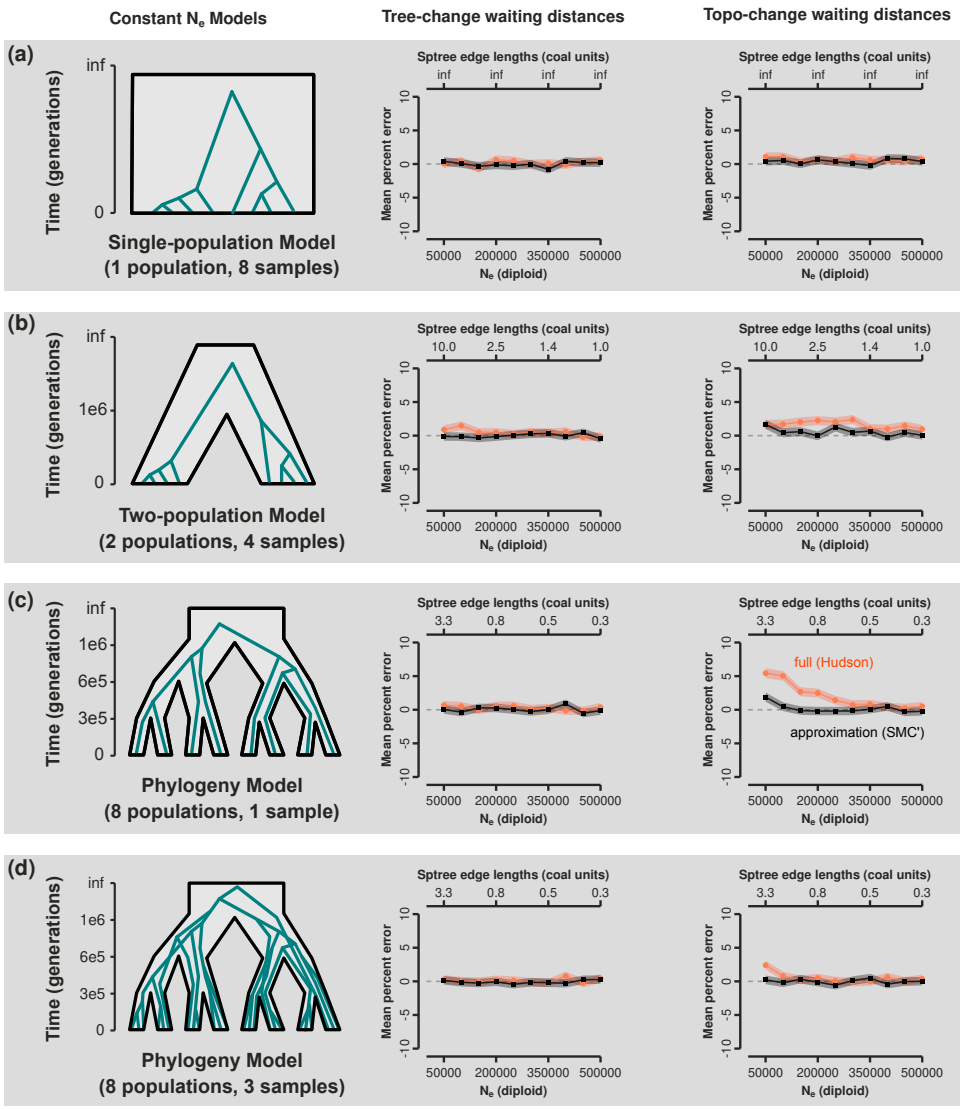

Figure S3. Error in the expected waiting distances to tree or topology-change events calculated under the MS-SMC. Error was measured as (observed - expected) / expected, where observed is the spanning distance of the first genealogy in a tree sequence until the next tree or topology-change event, and expected is the predicted waiting distance for the first genealogy until each event type given its embedding in the species tree model. Tree sequences were simulated for different demographic models across a range of parameter settings for N_e, and under two different ancestry models (SMC'=black; full coalescent with recombination (Hudson)=orange). (a-d) Estimated tree-change waiting distances exhibit very little error across all models and parameters tested. Estimated topology-change waiting distances exhibit elevated error at low N_e values in highly structured models, when the probability of a topology-change event is very low. (c) The error between analytical predictions and simulated data was greatest when the data were simulated under the full coalescent with recombination. (d) When more genomes are sampled per lineage the magnitude of error is greatly reduced.

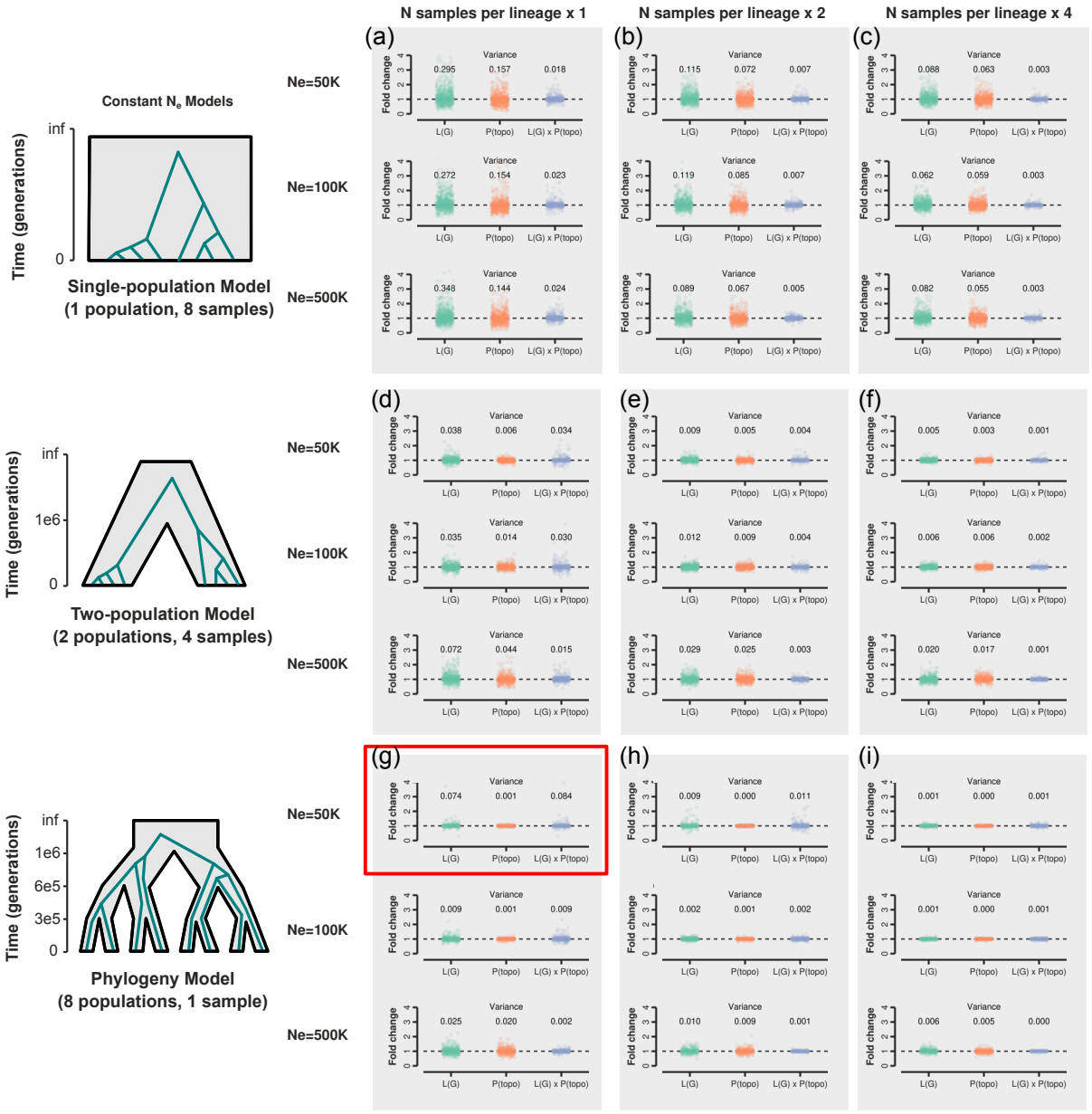

Figure S4. Variation between the first and second genealogies within topology-change intervals, and its impact on estimated waiting distances. Results are shown for 1K tree sequences simulated across a range of demographic models, N_e values, and numbers of genomes sampled per lineage. For each scenario, plots show the distribution of fold-change differences between the first and second genealogies in summed edge lengths (L(G)), the probability of a topology change (P(topo)), and the product of these metrics. The variance is shown above each distribution. (a-c) Single population demographic models consistently show high variance in the fold-change of each individual metric, but low variance in the fold-change of the product. (d-i) The two-population and phylogeny models typically exhibit less variance, except in the lowest N_e scenarios (e.g., red rectangle), where the product sometimes exhibits higher variance in fold-change. This suggests that the potential for tree-change events occurring within a topology-change interval to bias estimates of the waiting distance to a topology-change, is only a concern in scenarios where topology-change events are very unlikely. (e,f,h,i) Sampling more genomes per lineage greatly reduces this bias.

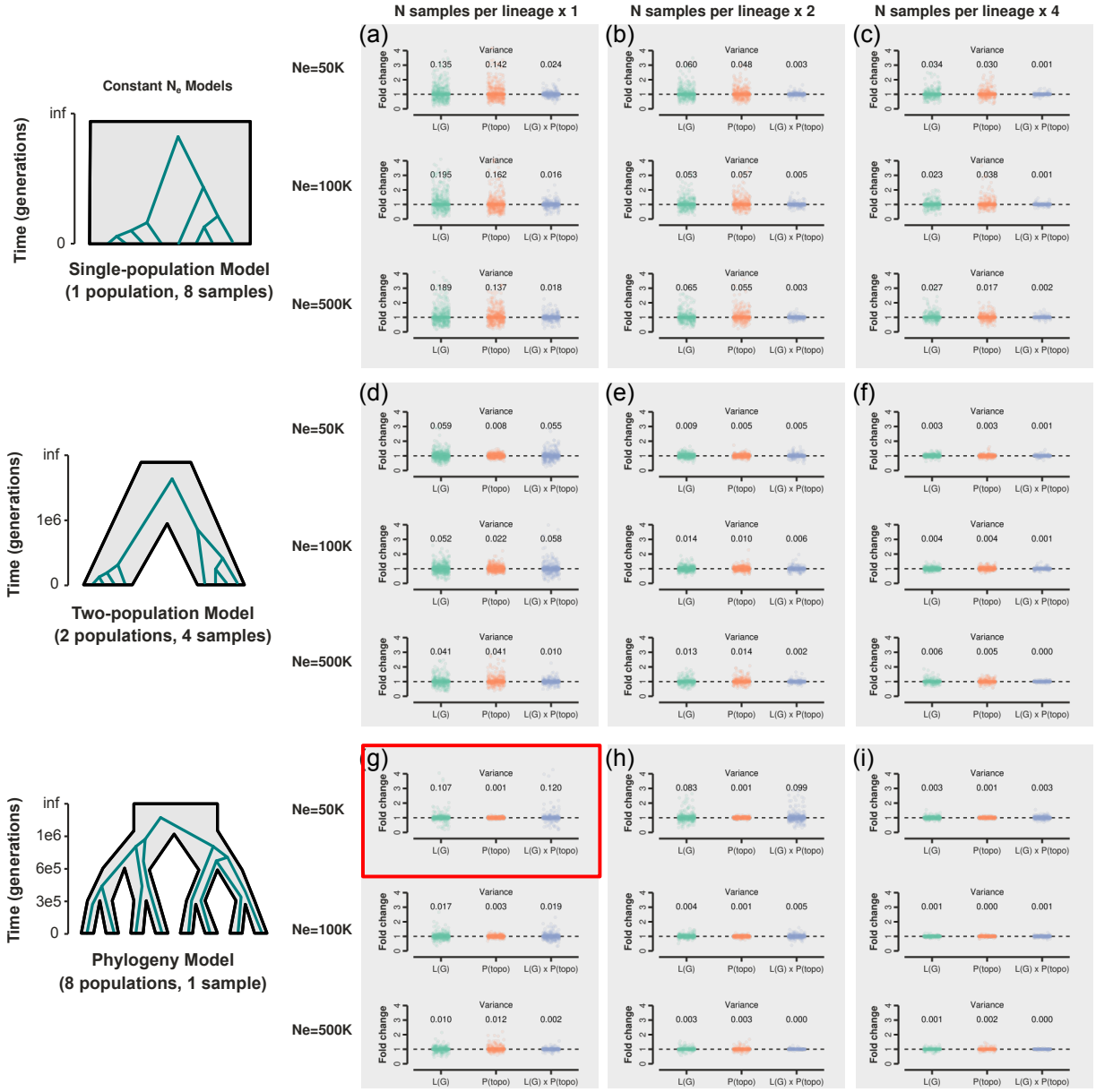

Figure S5. Variation between the first and last genealogies within topology-change intervals, and its impact on estimated waiting distances. Results are shown for 1K tree sequences simulated across a range of demographic models, N_e values, and numbers of genomes sampled per lineage. For each scenario, plots show the distribution of fold-change differences between the first and last genealogies in summed edge lengths (L(G)), the probability of a topology change (P(topo)), and the product of these metrics. The variance is shown above each distribution. (a-c) Single population demographic models consistently show high variance in the fold-change of each individual metric, but low variance in the fold-change of the product. (d-i) The two-population and phylogeny models typically exhibit less variance, except in the lowest N_e scenarios (e.g., red rectangle), where the product sometimes exhibits higher variance in fold-change. This suggests that the potential for tree-change events occurring within a topology-change interval to bias estimates of the waiting distance to a topology-change, is only a concern in scenarios where topology-change events are very unlikely. (e,f,h,i) Sampling more genomes per lineage greatly reduces this bias.

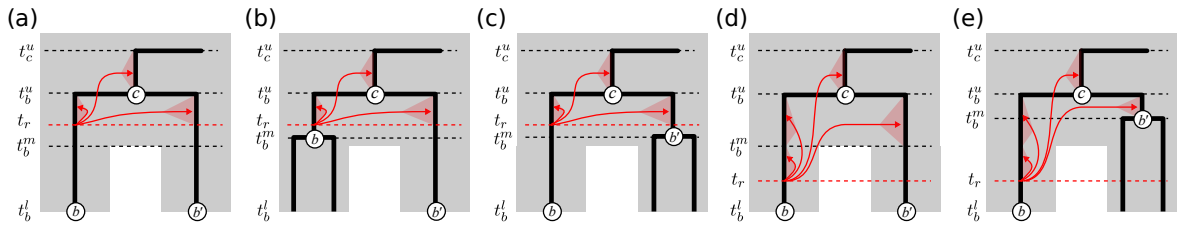

Figure S6. Calculating the probability that recombination on genealogy branch b leads to a topology change involves summing over the probabilities that the detached lineage does not re-coalesce with either itself, its sibling, or its parent (b, b' or c, respectively). The possibility of a tree-change outcome (e.g., shortened coalescent time) is restricted until the lowest shared interval between b and b', designated at time t_m. Opportunities for such events could be constrained by species divergences – as in (a) and (d) – or by the timing of prior coalescence events generating each branch – as in (b), (c), and (e). The possibility that recombination (t_r) occurs prior to t_m leads to the two ordered sets of intervals used in equations 11 and 12.

Table S1. Summary of variables used in waiting distance equations.

Variable	Description
$\mathcal{S}$	An MSC model with topology, divergence times and effective population sizes.
$\mathcal{G}$	A genealogy that can be embedded in $\mathcal{S}$.
$L(\mathcal{G})$	Sum of edge lengths of genealogy $\mathcal{G}$.
b	A focal branch in $\mathcal{G}$.
i	Interval in the genealogy embedding table in which recombination occurs.
$\mathcal{I}_b$	Ordered set of intervals on branch b.
$\mathcal{I}_c$	Ordered set of intervals on branch c, the parent of branch b.
$\mathcal{I}_{bc}$	Ordered union of sets $\mathcal{I}_b$ and $\mathcal{I}_c$.
$\mathcal{J}_b(i)$	Ordered set of intervals above i on branch b.
$\mathcal{Q}_b(i,j)$	Ordered set of intervals above i and below j on branch b.
$\mathcal{K}(b,t)$	Number of edges of $\mathcal{G}$ in the interval containing branch b at time t.
k_x	Number of edges of $\mathcal{G}$ in interval x; piece-wise constant of $A(b,t)$.
$\mathcal{N}(b,t)$	Diploid effective population size in the interval containing branch b at time t.
n_x	Diploid effective population size in interval x; piece-wise constant of $N(b,t)$.
t_r	Time of a recombination event, in generations.
σ_x	The lower boundary of interval x, in generations.
μ_x	The upper boundary of interval x, in generations.
d_x	The length of interval x, in generations.
t_b^l	The lower boundary of branch b, in generations.
t_b^u	The upper boundary of branch b, in generations.
t_b^m	The time at which a focal branch b is able to coalesce with its sibling branch.
$\mathcal{M}_b$	Ordered set of intervals above t_b^m on branch b.
$\mathcal{L}_b$	Ordered set of intervals below t_b^m on branch b.

Example: Calculating the probability of no-change

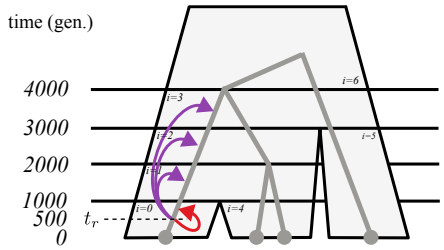

The probability of a no-change event given recombination on a specific branch at a specific time:

$$\mathbb{P}(\text{no-change}|\mathcal{S},\mathcal{G},b,t_r) = \frac{1}{k_i} + f(i,i)\exp\left\{\frac{k_i}{2n_i}t_r\right\} + \sum_{j\in\mathcal{J}_b(i)} f(i,j)\exp\left\{\frac{k_i}{2n_i}t_r\right\}$$

In this example, recombination occurs on branch *b* within interval 0 (*i*=0) at time t_r=500. Let's also assume, for this example that N_e=1000. Let's start by solving the constant ($\exp\left\{\frac{k_i}{2n_i}t_r\right\}$) which we can then assign to the variable X to make the equation much simpler.

$$\mathrm{X} = \exp\left\{\frac{k_i}{2n_i}t_r\right\} = \exp\left\{\frac{1}{2(1000)}500\right\} = 1.284$$

$$\mathbb{P}(\text{no-change}|\mathcal{S},\mathcal{G},b,t_r) = \frac{1}{k_i} + f(i,i)\,\mathrm{X} + \sum_{j\in\mathcal{J}_b(i)} f(i,j)\,\mathrm{X}$$

Next, we can substitute 0 for *i*, and define the set *J* of intervals on *b* above i as {1, 2, 3}. Also, we can solve $1/k_i$ which here is just 1. This gives the following:

$$\mathbb{P}(\text{no-change}|\mathcal{S},\mathcal{G},b,t_r) = 1 + f(0,0)\mathrm{X} + \sum_{j\in\{1,2,3\}} f(0,j)\,\mathrm{X}$$

All that is left to do is to expand the piecewise constant function *f(i,j)* for each interval and solve:

Equation: $f(i,i) = -\frac{1}{k_i}\exp\left\{-\frac{k_i}{2n_i}\mu_i\right\}$

With data: $f(0,0) = -\frac{1}{1}\exp\left\{-\frac{1}{2(1000)}1000\right\} = -0.6065$

Equation: $f(i,j) = \frac{1}{k_j}\left(1-\exp\left\{-\frac{k_j}{2n_j}d_j\right\}\right)\exp\left\{-\frac{k_i}{2n_i}\mu_i - \sum_{q\in\mathcal{Q}_b(i,j)}\frac{k_q}{2n_q}d_q\right\}$

With data: $f(0,1) = \frac{1}{3}\left(1-\exp\left\{-\frac{3}{2(1000)}1000\right\}\right)\exp\left\{-\frac{1}{2(1000)}1000\right\} = 0.1571$

$$f(0,2) = \frac{1}{2}\left(1-\exp\left\{-\frac{2}{2(1000)}1000\right\}\right)\exp\left\{-\frac{1}{2(1000)}1000 - \left(\frac{3}{2(1000)}1000\right)\right\} = 0.0428$$

$$f(0,3) = \frac{1}{3}\left(1-\exp\left\{-\frac{3}{2(1000)}1000\right\}\right)\exp\left\{-\frac{1}{2(1000)}1000 - \left(\frac{3}{2(1000)}1000 + \frac{2}{2(1000)}1000\right)\right\} = 0.0129$$

Finally, we sum the components to get the final result (colored to correspond with the figure above):

$$\begin{aligned}\mathbb{P}(\text{no-change}|\mathcal{S},\mathcal{G},b,t_r) &= 1 + f(0,0)\,\mathrm{X} + \sum_{j\in\{1,2,3\}} f(0,j)\,\mathrm{X} \\ &= 1 + (-0.6065 \times 1.284) + (0.1571 \times 1.284) + (0.0428 \times 1.284) + (0.0129 \times 1.284) \\ &= 0.4944\end{aligned}$$

Figure S7. A step-by-step calculation of the probability of a tree-unchanged event under the MS-SMC given a species tree and genealogy.

Example: Calculating the probability of topology-unchanged

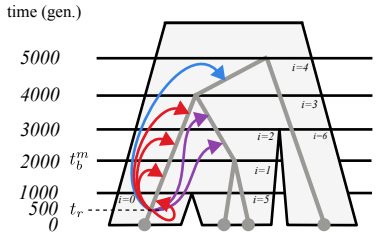

The probability of topology-unchanged given the branch and timing of recombination:

$$\mathbb{P}(\text{topology-unchanged}|\mathcal{S},\mathcal{G},b,t_r) = \begin{cases} \frac{1}{k_i} + \sum_{j\in\mathcal{I}_{bc}} f(i,j)\exp\left\{\frac{k_i}{2n_i}t_r\right\} + \sum_{j\in\mathcal{M}_b} f(i,j)\exp\left\{\frac{k_i}{2n_i}t_r\right\}, & \text{if } t_r < t_b^m \\ 2\left(\frac{1}{k_i} + \sum_{j\in\mathcal{I}_b} f(i,j)\exp\left\{\frac{k_i}{2n_i}t_r\right\}\right) + \sum_{j\in\mathcal{I}_c} f(i,j)\exp\left\{\frac{k_i}{2n_i}t_r\right\}, & \text{if } t_r \geq t_b^m \end{cases}$$

Because $t_r < t_b^m$, we will apply the first case. In this example, recombination occurs on branch *b* in interval 0 (*i*=0) at time t_r=500, and we will assume all N_e=1000. Let's start by solving the constant ($\exp\left\{\frac{k_i}{2n_i}t_r\right\}$) which we can then assign to the variable X to make the equation much simpler:

$$\mathrm{X} = \exp\left\{\frac{k_i}{2n_i}t_r\right\} = \exp\left\{\frac{1}{2(1000)}500\right\} = 1.284$$

$$\mathbb{P}(\text{topology-unchanged}|\mathcal{S},\mathcal{G},b,t_r) = \frac{1}{k_i} + \sum_{j\in\mathcal{I}_{bc}} f(i,j)\,\mathbf{X} + \sum_{j\in\mathcal{M}_b} f(i,j)\,\mathbf{X}$$

Next, we substitute 0 for *i*, and define the set of intervals (I_{bc}) over branch *b* and its parent as {0, 1, 2, 3, 4}, and define the set of intervals shared by *b* and its sister (M_b) as {2, 3}. Also, we can solve $1/k_i$ which here is just 1.

$$\mathbb{P}(\text{topology-unchanged}|\mathcal{S},\mathcal{G},b,t_r) = 1 + \sum_{j\in\{0,1,2,3,4\}} f(i,j)\,\mathbf{X} + \sum_{j\in\{2,3\}} f(i,j)\,\mathbf{X}$$

All that is left to do is to expand the piecewise constant function *f(i,j)* for each interval and solve:

Equation: $f(i,i) = -\frac{1}{k_i}\exp\left\{-\frac{k_i}{2n_i}\mu_i\right\}$

With data: $f(0,0) = -\frac{1}{1}\exp\left\{-\frac{1}{2(1000)}1000\right\} = -0.6065$

Equation: $f(i,j) = \frac{1}{k_j}\left(1-\exp\left\{-\frac{k_j}{2n_j}d_j\right\}\right)\exp\left\{-\frac{k_i}{2n_i}\mu_i - \sum_{q\in\mathcal{Q}_b(i,j)}\frac{k_q}{2n_q}d_q\right\}$

With data: $f(0,1) = \frac{1}{3}\left(1-\exp\left\{-\frac{3}{2(1000)}1000\right\}\right)\exp\left\{-\frac{1}{2(1000)}1000\right\} = 0.1571$

$f(0,2) = \frac{1}{2}\left(1-\exp\left\{-\frac{2}{2(1000)}1000\right\}\right)\exp\left\{-\frac{1}{2(1000)}1000-\left(\frac{3}{2(1000)}1000\right)\right\} = 0.0428$

$f(0,3) = \frac{1}{3}\left(1-\exp\left\{-\frac{3}{2(1000)}1000\right\}\right)\exp\left\{-\frac{1}{2(1000)}1000-\left(\frac{3}{2(1000)}1000+\frac{2}{2(1000)}1000\right)\right\} = 0.0129$

$f(0,2) = \frac{1}{2}\left(1-\exp\left\{-\frac{2}{2(1000)}1000\right\}\right)\exp\left\{-\frac{1}{2(1000)}1000-\left(\frac{3}{2(1000)}1000\right)\right\} = 0.0428$

$f(0,3) = \frac{1}{3}\left(1-\exp\left\{-\frac{3}{2(1000)}1000\right\}\right)\exp\left\{-\frac{1}{2(1000)}1000-\left(\frac{3}{2(1000)}1000+\frac{2}{2(1000)}1000\right)\right\} = 0.0129$

$f(0,4) = \frac{1}{2}\left(1-\exp\left\{-\frac{2}{2(1000)}1000\right\}\right)\exp\left\{-\frac{1}{2(1000)}1000-\left(\frac{3}{2(1000)}1000+\frac{2}{2(1000)}1000+\frac{3}{2(1000)}1000\right)\right\} = 0.0035$

Finally, we sum the components to get the final result (colored to correspond with the figure above):

$= 1+(-0.6065\times1.284)+(0.1571\times1.284)+(0.0428\times1.284)+(0.0129\times1.284)+(0.0035\times1.284)+(0.0428\times1.284)+(0.0129\times1.284)$

$= 0.5703$

Figure S8. A step-by-step calculation of the probability of a topology-unchanged event under the MS-SMC given a species tree and genealogy.

5.2 Investigating bias in MS-SMC predictions

The MS-SMC harbors two potential sources of bias, the first stemming from assumptions of the SMC' approximation and the second from the potential inhomogeneity among genealogies that can exist between topology-change events. We examined both of these sources of error through comparison to stochastic simulations and found that their effects are generally negligible, and that structured demographic models do not exhibit greater error than a single-population model under most scenarios.

5.2.1 Bias associated with the SMC' approximation

To investigate the extent to which the SMC' approximation leads to errors in waiting distance estimation, we repeated the simulations from our validation scenario using the SMC' model (msprime setting "ancestry_model=smc_prime") as opposed to the full coalescent with recombination model ("ancestry_model=hudson") that we used previously. We expect that waiting distances in simulations under the SMC' will match our analytical predictions more closely than the waiting distances in simulations under the full coalescent with recombination, since our MS-SMC model relies on the assumptions of the SMC'. For each simulated tree sequence we calculated the expected waiting distance to a tree or topology-change event given the starting genealogy and species tree, and compared this to the observed waiting distance to each event type for the starting genealogy in the simulation. We measured the percent error for each genealogy as $100 \times$ (simulated waiting distance - expected waiting distance) / expected waiting distance. This was repeated across 100K tree sequences for each simulation setting, and the mean and standard error were calculated.

The error in our analytical predictions was very low across all demographic models and parameter settings tested, regardless of whether data were simulated under the SMC' approximation or not (Fig. S3). The mean percent error in estimated tree-change waiting distances rarely exceeded 1%, while the error in estimated topology-change waiting distances varied depending on the demographic and simulation models. The error in estimated topology-change waiting distances was always $<5\%$ for data simulated under the SMC', and only exceeded 5% in one scenario tested for simulations under the full coalescent with recombination. This scenario represents an extreme case, in the form of a "Phylogeny Model" with only a single sample per species, and very low Ne, such that genealogical discordance is very low. This leads to very long expected waiting distances between topology events, and very high variance in the simulated outcomes (Fig. S3c). By simply increasing the number of samples per lineage, such that topology-change events can occur not only between lineages, but also within them, this error is reduced to approximately 2% for the full coalescent with recombination, and nearly zero for SMC' data (Fig. S3d).

Although tree-change waiting distances did not exhibit consistent errors, the error in estimated topology-change waiting distances, when present, was consistently in the direction of being under-estimated. The fact that this bias is not observed in the distance to tree-change events, but only for topology-change events, suggests that the SMC' approximation has little effect on the accuracy of estimation for an individual genealogy, but can lead to more detectable errors when compounded over many tree-change events occurring between a topology-change event. In other words, the SMC' approximation does not introduce a significant bias on its own, but does contribute to increased error in topology-change change waiting distances through its interaction with a second source of error, the inhomogeneity of genealogies between topology-

change events (examined further below). We expect that the reason this bias tends to occur in the direction of under-estimated waiting distances to a topology-change is because the intervening tree-change events can cause the genealogy to enter a space where the probability of a topology-change is much less likely than it was on the tree at the start of the interval.

5.2.2 Bias associated with inhomogeneity between topology-change events

To investigate the impact of genealogical variation within a topology-change interval on the accuracy of its estimated waiting distance, we measured how much genealogies vary within these intervals, and how much this impacts probabilities of topology-change. Because topology-change waiting distances are calculated based on the genealogy at the start of an interval, we compared the first genealogy to both the second and last genealogy in each interval. For each tree we calculated the genealogy length ($L(\mathcal{G})$), the probability of a topology-change given $\mathcal{G}$ and $\mathcal{S}$, and the product of these two metrics, which equates to the waiting distance rate parameter (equations 7, 8, 10). Deng *et al.* (2021) noted that for a single population with constant N_e there is an inverse relationship between genealogy length and the probability of a topology change, such that their product exhibits little variation even if genealogies vary across an interval. It was not clear whether this is also true for an MSC model, since the embedding of a genealogy into the species tree affects the probability of a topology change in addition to the edge lengths of the genealogy.

Therefore, we examined genealogical variation across three demographic models, at three different values for N_e, and for different numbers of genomes sampled per population. We simulated 1,000 tree sequences for each scenario using the coalescent with recombination ancestry model. For each tree sequence we extracted information from one topology-change interval. To select the interval we advanced to the first interval after the first topology-change event that included at least one tree-change event within it. For this interval we measured $L(\mathcal{G})$, $\mathbb{P}(\text{topology-change}|\mathcal{S},\mathcal{G})$ and their product, for the first genealogy, second genealogy, and last genealogy in the interval. We measured the fold-change for each variable between the first and second genealogies, and between the first and last genealogies.

Across all simulations our results confirm and extend the conclusions of Deng *et al.* (2021), showing that although $L(\mathcal{G})$ and $\mathbb{P}$ can both exhibit high variance in fold-change between the first and second genealogies in an interval (Fig. S4), and between the first and last genealogies in an interval (Fig. S5), the product of these two metrics almost always exhibits lower variance in fold-change, and is centered on one. In a single population model the variance in the fold-change of the product of these two metrics was approximately 0.02, and did not vary with N_e, or depending on whether we compared the first and second, or first and last trees in an interval. The variance in the product was reduced by nearly an order of magnitude when the number of genomes sampled was increased (Fig. S4a-c,S5a-c). We can conclude that genealogical heterogeneity has a very small effect on estimated waiting distances to topology-changes in a single population model.

In the two-population and phylogeny models the variance in the fold change of $L(\mathcal{G})$, $\mathbb{P}$, and their product was strongly affected by the model N_e, and consistently smaller between the first and second genealogy, than between the first and last genealogy in an interval. (Fig. S4d-i,S5d-i). Despite this, the variance in fold-change of the product was of a similar magnitude or lower than in the single-population model across nearly all of the multi-species scenarios tested. The only exception is the extreme case noted previously, representing the Phylogeny Model with only a single genome sampled per tip, examined at the

lowest N_e value (50K), where the probability of a topology-change is very low because the probability of coalescence within each species tree interval is very high (Fig. S4g,S5g). At only slightly higher values of N_e (100K) the variance in the fold-change difference between trees is of a similar magnitude, or lower, than that seen in the single population model. Thus, we can conclude that genealogical heterogeneity has only a small effect on estimated waiting distances to topology-changes in most multi-species coalescent models, but that care should be taken when interpreting MS-SMC estimated waiting distances to topology-changes estimated on datasets that lack genealogical discordance. As noted previously, simply increasing the number of sampled genomes per lineage, to a number that allows topology-change events to occur both within and between lineages, reduces the variation in topology-change probabilities across within intervals to negligible values (Fig. S4i,S5i).

6 Appendix: Derivations

6.1 Notation

Information from the genealogy embedding table (described in the following paragraph) can be used in equations that calculate the probabilities of no-change, tree-change, and topology-change events under the MS-SMC. These equations, described throughout rest of the Appendix, use the terms defined in Table S1. A parameterized species tree, $\mathcal{S}$, is a multispecies coalescent model in which a set of isolated populations are related by a bifurcating tree topology. Divergence times between lineages are in units of generations, and each edge (species tree interval) can be associated with a different constant diploid effective population size (N_e). A genealogy, $\mathcal{G}$, represents the genealogical relationships – composing a topology and coalescent times in units of generations – for a set of sampled gene copies at some position in their genomes. A genealogy can be embedded in a species tree if the coalescent times between sampled gene copies from different populations are not younger than a population divergence event separating them.

Given a genealogy embedded in a species tree, a series of discrete time intervals can be defined that are delimited by events that change the rate of coalescence. We refer to this set of discrete time intervals and their associated properties as a genealogy embedding table (e.g., Fig. 2b). In the waiting distance solutions for a single population with constant N_e by Deng *et al.* (2021), this table is delimited only by coalescent events, and the intervals are non-overlapping. Because N_e is constant in their framework, only k differs between intervals. Therefore, changes in k alone determine differences in rates of coalescence, with k decreasing monotonically in subsequent intervals from the tips towards the root. Our approach is similar, but adds additional complexity (Fig. 4). In the multispecies framework, genealogy embedding intervals are specific to each species tree branch, with each one corresponding to a time interval with a constant k and N_e in a specific species tree branch. Breakpoints between intervals arise where divergences occur in the species tree (increasing k and potentially changing N_e) and where coalescent events occur in the genealogy (reducing k). Genealogy embedding intervals corresponding to different species tree branches can overlap in time.

Each branch on $\mathcal{G}$ will span one or more genealogy embedding intervals. The ordered set of intervals on a specific branch, b, is defined as $\mathcal{I}_b$. The lower and upper time bounding each interval is σ_x and μ_x, respectively, where x is the index of the interval in the genealogy embedding table. The lower and upper bounds of each branch are defined as t_b^l and t_b^u, respectively.

6.2 Extending SMC' waiting distance solutions:

The probabilities of different recombination event types under the MS-SMC are calculated from the probability that recombination occurs on a specific branch and the probabilities that the resulting detached subtree subsequently re-coalesces with any other available branch above that time. The opportunity for recombination to occur on a branch is scaled by its length in generations (t_b^u - t_b^l). Similarly, the probability of re-coalescence on a branch is scaled by its length and the coalescence rate. The latter can vary over the length of a branch as it spans different intervals, and is a function of the effective population size in the species tree interval that includes branch b at a specified time, τ, defined as $\mathcal{N}(b, \tau)$, and the number of other genealogy branches in the interval that includes branch b at time τ, defined as $\mathcal{K}(b, \tau)$. Finally, the probability that coalescence occurs over an interval of length (t) can be calculated from an exponential probability density $f(t; \lambda)$, where the rate parameter is $\lambda = \frac{\mathcal{K}(b,\tau)}{2\mathcal{N}(b,\tau)}$, similar to equations 1-2.

6.3 Probability of no-change

6.3.1 Given a branch and time of recombination

The probability that a tree is unchanged by a recombination event – meaning that no coalescent times are changed – is the probability that the detached subtree re-coalesces with the same branch it detached from. Thus, we can integrate from the time of recombination (t_r) to the top of the branch (t_b^u) over the probability of sampling the same branch times the exponential probability density of re-coalescing at any time on that branch above the time of recombination ($\tau - t_r$). We take this integral with respect to τ, where $\mathcal{K}(b, \tau)$ and $\mathcal{N}(b, \tau)$ can vary across the length of the branch if it spans different intervals.

$$\mathbb{P}(\text{tree-unchanged}|\mathcal{S}, \mathcal{G}, b, t_r) = \int_{t_r}^{t_b^u} \frac{1}{\mathcal{K}(b,\tau)} f(\tau - t_r; \lambda) d\tau \tag{S1}$$

The exponential probability density function can be expanded, as in equation 2, where λ is $\mathcal{K}(b, \tau)$ over $2\mathcal{N}(b, \tau)$:

$$= \int_{t_r}^{t_b^u} \frac{1}{\mathcal{K}(b,\tau)} \frac{\mathcal{K}(b,\tau)}{2\mathcal{N}(b,\tau)} \exp\left\{ - \int_{t_r}^{\tau} \frac{\mathcal{K}(b,s)}{2\mathcal{N}(b,s)} ds \right\} d\tau \tag{S2}$$

This simplifies to the following equation, which describes the probability that the subtree re-coalesces at any time ($d\tau$) on b above t_r, and that it does not re-coalesce at any intervening time (ds) between t_r and τ.

$$= \int_{t_r}^{t_b^u} \frac{1}{2\mathcal{N}(b,\tau)} \exp\left\{ - \int_{t_r}^{\tau} \frac{\mathcal{K}(b,s)}{2\mathcal{N}(b,s)} ds \right\} d\tau \tag{S3}$$

Because the rate of re-coalescence is constant within each interval, we next split this equation into statements over each discrete interval that the detached subtree could possibly re-coalesce with on branch b. (Recall, because we are currently computing the probability of a no-change event we only need to concern ourselves with re-coalescence on branch b.) Here, the interval in which recombination occurred on branch b is labeled as i.

In the equation below, the first integral describes the probability statement over only part of interval i, from t_r to u_i, rather than over its entire length, since re-coalescence can only occur above the time at

which recombination occurred. By contrast, the latter parts of this equation are performed over the entire lengths of each remaining interval above i, from the bottom (σ_j) to the top (μ_j) of the interval. The ordered set of all intervals above i in $\mathcal{I}_b$ is defined as $\mathcal{J}_b(i) = \{j \in \mathcal{I}_b \mid j > i\}$.

$$= \int_{t_r}^{\mu_i} \frac{1}{2\mathcal{N}(b,\tau)} \exp\left\{ -\int_{t_r}^{\tau} \frac{\mathcal{K}(b,s)}{2\mathcal{N}(b,s)} ds \right\} d\tau + \sum_{j \in \mathcal{J}_b(i)} \int_{\sigma_j}^{\mu_j} \frac{1}{2\mathcal{N}(\tau)} \exp\left\{ -\int_{t_r}^{\tau} \frac{\mathcal{K}(s)}{2\mathcal{N}(s)} ds \right\} d\tau \quad \text{(S4)}$$

We can now solve this equation and substitute constant values for $\mathcal{K}(b,\tau)$ and $\mathcal{N}(b,\tau)$ in each interval. Because the first term is computed over only part of the first interval we first solve this term separately, and then show the result for the later terms. The first term concerns the probability of re-coalescing in the same interval i in which recombination occurred. The center part of this equation will appear again later, and so we define it as the function $f(i,i)$.

$$= \frac{1}{k_i} - \frac{1}{k_i} \exp\left\{ -\frac{k_i}{2n_i} \mu_i \right\} \exp\left\{ \frac{k_i}{2n_i} t_r \right\} \quad \text{(S5)}$$

$$= \frac{1}{k_i} + f(i,i) \exp\left\{ \frac{k_i}{2n_i} t_r \right\} \quad \text{(S6)}$$

We similarly define the function $f(i,j)$ for the later terms in this equation, which refer to the probability of re-coalescing in a later interval, j, than the one in which recombination occurred, i. This function requires also summing over any intervening intervals, q. For this, we define the function $\mathcal{Q}_b(i,j) = \{q \in \mathcal{I}_b \mid j > q > i\}$ to return the ordered set of intervals on branch b between i and j:

$$= \sum_{j \in \mathcal{J}_b(i)} \frac{1}{k_j} \left(1 - \exp\left\{ -\frac{k_j}{2n_j} d_j \right\} \right) \exp\left\{ -\frac{k_i}{2n_i} \mu_i - \sum_{q \in \mathcal{Q}_b(i,j)} \frac{k_q}{2n_q} d_q \right\} \exp\left\{ \frac{k_i}{2n_i} t_r \right\} \quad \text{(S7)}$$

$$= \sum_{j \in \mathcal{J}_b} f(i,j) \exp\left\{ \frac{k_i}{2n_i} t_r \right\} \quad \text{(S8)}$$

The $f(i,i)$ and $f(i,j)$ function above is represented in the main text as equation 4. Adding the two terms that include these functions together we get equation 3 from the main text for the probability of a no-change event given the timing and branch on which recombination occurs:

$$\mathbb{P}(\text{no-change} | \mathcal{S}, \mathcal{G}, b, t_r) = \frac{1}{k_i} + f(i,i) \exp\left\{ \frac{k_i}{2n_i} t_r \right\} + \sum_{j \in \mathcal{J}_b(i)} f(i,j) \exp\left\{ \frac{k_i}{2n_i} t_r \right\} \quad (3)$$

Note that in equation 3 above, while we have split the terms for clarity, the $f(i,i)$ term could be lumped into the summation. The summation would then be indexed using $j \in \mathcal{I}_b$, with the understanding that $f(i,j) = 0$ when $i > j$ – that is, when summing over intervals that fall below the time of recombination.

6.3.2 Across a full branch

Having solved for the probability of the genealogy being unchanged given the time t_r of the recombination event, our next step is to integrate this equation across the entire branch with respect to t_r:

$$\mathbb{P}(\text{tree-unchanged}|\mathcal{S},\mathcal{G},b) = \frac{1}{t_b^u - t_b^l}\int_{t_b^l}^{t_b^u} \mathbb{P}(\text{tree-unchanged}|\mathcal{S},\mathcal{G},b,t_r)dt_r \tag{S9}$$

Plugging in the piece-wise constant solutions from equation 3 we get the following solution.

$$\begin{aligned} &= \frac{1}{t_b^u - t_b^l}\sum_{i\in\mathcal{I}_b}\frac{1}{k_i}d_i + \left(\exp\left\{\frac{k_i}{2n_i}\mu_i\right\} - \exp\left\{\frac{k_i}{2n_i}\sigma_i\right\}\right) \\ &\left[-\frac{2n_i}{k_i^2}\exp\left\{-\frac{k_i}{2n_i}\mu_i\right\}+\right. \\ &\left.\frac{2n_i}{k_i}\left(\sum_{j\in\mathcal{J}_b(i)}\exp\left\{-\frac{k_i}{2n_i}\mu_i - \sum_{q\in\mathcal{Q}_b(i,j)}\frac{k_q}{2n_q}d_q\right\}\frac{1}{k_j}\left(1-\exp\left\{-\frac{k_j}{2n_j}d_j\right\}\right)\right)\right] \end{aligned} \tag{S10}$$

Finally, this can be simplified to the following solution by expressing the piecewise constant re-coalescence rates using the function $f(i,j)$, as shown in equation 5 from the main text.

$$\mathbb{P}(\text{tree-unchanged}|\mathcal{S},\mathcal{G},b) = \frac{1}{t_b^u - t_b^l}\int_{t_b^l}^{t_b^u} \mathbb{P}(\text{tree-unchanged}|\mathcal{S},\mathcal{G},b,t)dt$$

$$= \frac{1}{t_b^u - t_b^l}\sum_{i\in\mathcal{I}_b}\left[\frac{1}{k_i}d_i + \left(\frac{2n_i}{k_i}\sum_{j\in\mathcal{I}_b}f(i,j)\left(\exp\left\{\frac{k_i}{2n_i}\mu_i\right\} - \exp\left\{\frac{k_i}{2n_i}\sigma_i\right\}\right)\right)\right] \tag{5}$$

6.3.3 Across the whole tree

At last, we can calculate the probability that, given a recombination event, the genealogy is unchanged. We do this by weighting each branch by its proportion of the total tree length and summing across the unchanging probabilities for all branches. This is equation 6 from the main text:

$$\mathbb{P}(\text{tree-unchanged}|\mathcal{S},\mathcal{G}) = \sum_{b\in G}\left[\frac{t_b^u - t_b^l}{L(\mathcal{G})}\right]\mathbb{P}(\text{tree-unchanged}|\mathcal{S},\mathcal{G},b) \tag{6}$$

We can then also derive the probability of a tree-change event as $1 - \mathbb{P}(\text{tree-unchanged}|\mathcal{S},\mathcal{G})$. Following the approach described in equations 7-10, we can then calculate an exponential probability distribution for waiting distances between no-change or tree-change events using an exponential rate parameter that is scaled by the probabilities of either recombination event type.

6.4 Probability of topology change

Next, we derive the probability of a topology-unchanged event, from which we can get the associated probability of a topology-change event. As in the first section, we first derive a solution given an individual branch and time of recombination. We then extend this solution to an entire branch, and we finally sum across branches to get a probability for the entire genealogy. To isolate events that do not cause a topology change, we must find the union of events that cause a no-change event in addition to two types of possible tree-change events which affect only branch lengths but not the topology. These two types of events correspond to a re-coalescence with the sibling to branch b, termed b', or with its parent, c (Fig. 3d). Because

branch c is always ancestral to b, a recombination event on b can potentially re-coalesce anywhere on c; however, this is not the case for b', which may only exist or be available for re-coalescence over part of the length of b. It is therefore important to define the lowest time point at which re-coalescence with b' is possible, termed t_b^m.

In the single population model of Deng *et al.* (2021), t_b^m occurs at the maximum value of t_b^l and $t_{b'}^l$, representing the lower bounds of b and b', respectively. In our MSC-based model we must also incorporate potential constraints imposed by population barriers, and so t_b^m occurs at the maximum of t_b^l, $t_{b'}^l$, and any population divergence events that separate b and b' (Fig. S6a-c).

6.4.1 Given a branch and time of recombination

Using the definition for t_b^m from above, we can describe the probability of a topology-unchanged event given the branch and time of recombination as a two-part solution. These two parts correspond to scenarios in which the time of recombination, t_r, occurs either above (Fig. S6a-c) or below (Fig. S6d-e) t_b^m. When $t_r >= t_b^m$, there are only two distinct intervals over which re-coalescence can occur: from t_r to t_b^u on branches b or b', and from t_b^u to t_c^u on branch c (Fig. S6a-c). By contrast, when $t_r < t_b^m$ there are three distinct intervals for re-coalescence: from t_r to t_b^m on b, t_b^m to t_b^u on b or b', and t_b^u to t_c^u on branch c (Fig. S6d-e). Thus, in the first scenario the opportunity for re-coalescence is the same for branches b and b', whereas in the latter scenario it is different.

Retaining the correct order of intervals is important in these calculations, particularly for $f(i,j)$, which involves summing over not only the information in the i and j intervals, but also all of the intervals that lie between them. To iterate over ordered intervals on each branch we define additional indexing variables. Just as $\mathcal{I}_b$ defines the ordered set of intervals on branch b, $\mathcal{I}_c$ is the ordered set of intervals on branch c, and $\mathcal{I}_{bc}$ is the ordered union of these sets. In addition, we define $\mathcal{M}_b$ as the ordered intervals on branch b above t_b^m, and $\mathcal{L}_b$ as the ordered intervals on branch b below t_b^m. We can now derive a probability for the two distinct scenarios:

First case – Given $t_r < t_b^m$, we integrate over the three distinct intervals where re-coalescence can occur. The first is unique to branch b, the second integral is multiplied by two since from t_b^m to t_b^u re-coalescence can occur with b or b', and the final integral is over the length of branch c. By substituting the piece-wise constant solutions for each interval into this equation it can be simplifed to the final form below, also shown in equation 11 of the main text:

$$\begin{aligned}
&\mathbb{P}(\text{topology-unchanged}|\mathcal{S},\mathcal{G},b,t_r) \\
&= \int_{t_r}^{t_b^m} \frac{1}{\mathcal{K}(b,\tau)} f(\tau - t_r;\lambda)d\tau + \int_{t_b^m}^{t_b^u} \frac{2}{\mathcal{K}(b,\tau)} f(\tau - t_r;\lambda)d\tau + \int_{t_b^u}^{t_c^u} \frac{1}{\mathcal{K}(b,\tau)} f(\tau - t_r;\lambda)d\tau \\
&= \frac{1}{k_i} + \sum_{j\in\mathcal{I}_{bc}} f(i,j)\exp\left\{\frac{k_i}{2n_i}t_r\right\} + \sum_{j\in\mathcal{M}_b} f(i,j)\exp\left\{\frac{k_i}{2n_i}t_r\right\}
\end{aligned} \tag{S11}$$

Second case – Given $t_r >= t_b^m$, we only need to integrate over two distinct intervals, thus we simply drop the first term from the equation above. The final form of this equation is also shown in equation 11 of

the main text:

$$\begin{aligned}
&\mathbb{P}(\text{topology-unchanged}|\mathcal{S},\mathcal{G},b,t_r)\\
&=\int_{t_r}^{t_b^u}\frac{2}{\mathcal{K}(b,\tau)}f(\tau-t_r;\lambda)d\tau+\int_{t_b^u}^{t_c^u}\frac{1}{\mathcal{K}(b,\tau)}f(\tau-t_r;\lambda)d\tau\\
&=2\left(\frac{1}{k_i}+\sum_{j\in\mathcal{I}_b}f(i,j)\exp\left\{\frac{k_i}{2n_i}t_r\right\}\right)+\sum_{j\in\mathcal{I}_c}f(i,j)\exp\left\{\frac{k_i}{2n_i}t_r\right\}
\end{aligned}\tag{S12}$$

6.4.2 Across a full branch

Now we derive the overall probability that a recombination event falling on a specific branch will not change the topology by integrating across the range of possible values for t_r. Following the approach above, we split this problem into two parts, above and below t_b^m, and we sum the two cases.

$$\mathbb{P}(\text{topology-unchanged}|\mathcal{S},\mathcal{G},b)=\frac{1}{t_b^u-t_b^l}\int_{t_b^l}^{t_b^u}\mathbb{P}(\text{topology-unchanged}|\mathcal{S},\mathcal{G},b,t_r)dt_r \tag{S13}$$

$$=\frac{1}{t_b^u-t_b^l}\left[\left(\int_{t_b^l}^{t_b^m}+\int_{t_b^m}^{t_b^u}\right)\mathbb{P}(\text{topology-unchanged}|\mathcal{S},\mathcal{G},b,t_r)dt_r\right] \tag{S14}$$

First case – We can simply sum over each entire interval below t_b^m where t_r could occur, and substitute piece-wise constant solutions for the probabilities that a detached subtree will re-coalesce over the subset of targeted intervals above this that do not cause a topology-change.

$$\begin{aligned}
&\int_{t_b^l}^{t_b^m}\mathbb{P}(\text{topology-unchanged}|\mathcal{S},\mathcal{G},b,t_r)dt_r\\
&=\sum_{i\in\mathcal{L}_b}\frac{1}{k_i}\left[d_i+2n_i\left(\exp\left\{\frac{k_i}{2n_i}\mu_i\right\}-\exp\left\{\frac{k_i}{2n_i}\sigma_i\right\}\right)\left(\sum_{j\in\mathcal{I}_{bc}}f(i,j)+\sum_{j\in\mathcal{M}_b}f(i,j)\right)\right]
\end{aligned}\tag{S15}$$

Second case – Similarly, we can sum over each entire interval above t_b^m (up to t_b^u) and substitute piece-wise constant solutions for the same selected subset of intervals:

$$\begin{aligned}
&\int_{t_b^m}^{t_b^u}\mathbb{P}(\text{topology-unchanged}|\mathcal{S},\mathcal{G},b,t_r)dt_r\\
&=\sum_{i\in\mathcal{M}_b}\frac{1}{k_i}\left[2d_i+2n_i\left(\exp\left\{\frac{k_i}{2n_i}\mu_i\right\}-\exp\left\{\frac{k_i}{2n_i}\sigma_i\right\}\right)\left(2\sum_{j\in\mathcal{I}_b}f(i,j)+\sum_{j\in\mathcal{I}_c}f(i,j)\right)\right]
\end{aligned}\tag{S16}$$

Result – If we express the inner summed terms from the equations above, composed of piece-wise constant values from their intervals, as $p_{b,1}^{(i)}$ and $p_{b,2}^{(i)}$, respectively, then the final solution can be expressed more concisely. This is shown in the main text as equation 12.

$$\mathbb{P}(\text{topology-unchanged}|\mathcal{S},\mathcal{G},b) = \frac{1}{t_b^u - t_b^l}\left[\sum_{i\in\mathcal{L}_b} p_{b,1}^{(i)} + \sum_{i\in\mathcal{M}_b} p_{b,2}^{(i)}\right] \tag{12}$$

6.4.3 Across the whole tree

Finally, we sum across all branches, each weighted by their relative length, to find the probability of a recombination event not changing the topology of the tree. This appears as equation 13 in the main text.

$$\begin{aligned}\mathbb{P}(\text{topology-unchanged}|\mathcal{S},\mathcal{G}) &= \sum_{b\in\mathcal{G}} \frac{t_b^u - t_b^l}{L(\mathcal{G})} \times \mathbb{P}(\text{topology-unchanged}|\mathcal{S},\mathcal{G},b) \\ &= \frac{1}{L(\mathcal{G})}\sum_{b\in\mathcal{G}}\left[\sum_{i\in\mathcal{L}_b} p_{b,1}^{(i)} + \sum_{i\in\mathcal{M}_b} p_{b,2}^{(i)}\right]\end{aligned} \tag{13}$$

6.4.4 Examples

Examples showing how to compute the probability of a no-change (tree-unchanged) or topology-unchanged event are shown with didactic step-by-step instructions in Fig. S7 and Fig. S8, respectively.